2010

Design Of A Wideband Dual-polarized Cavity Backed Slot Antenna

Rajesh Paryani
University of Central Florida

DESIGN OF A WIDEBAND DUAL-POLARIZED CAVITY BACKED SLOT ANTENNA

by

RAJESH C PARYANI
M.S. University of Central Florida, 2008

A dissertation submitted in partial fulfillment of the requirements
for the degree of Doctor of Philosophy
in the School of Electrical Engineering and Computer Science
in the College of Engineering & Computer Science
at the University of Central Florida
Orlando, Florida

Spring Term
2010

Major Professors:
Parveen F Wahid
Nader Behdad

ABSTRACT

A new technique for designing wideband dual-polarized cavity-backed slot antennas is presented. The structure is in the form of a double-resonant, dual-polarized slot antenna backed by a shallow substrate integrated cavity with a depth of approximately $\lambda_0/10$, where λ_0 is the wavelength in free space. The presence of the cavity behind the slot enhances the antenna's directivity and reduces the possibility of surface wave propagation in the antenna substrate when the element is used in an array environment. Moreover, the dual-polarized nature of this radiating element may be exploited to synthesize any desired polarization (vertical, horizontal, RHCP, or LHCP). The double-resonant behavior observed in this substrate-integrated cavity-backed slot antenna (SICBSA) is utilized to enhance its bandwidth compared to a typical cavity-backed slot antenna. A prototype of the proposed antenna is fabricated and tested. Measurement results indicate that a bandwidth of 19%, an average gain of 5.3 dB, and a wideband differential isolation of 30 dB can be achieved using this technique. The principles of operation along with the measurement results of the fabricated prototype are presented and discussed in this dissertation.

The SICBSA is investigated as a candidate for use as an array element. A uniform two element phased array is demonstrated to locate the main beam from boresight to thirty degrees. The potential effects of mutual coupling and surface wave propagation are considered and analyzed.

This dissertation is dedicated to my wife, Robyn, and my mother, Marianne, without whom I would be lost.

ACKNOWLEDGMENTS

Dr. Parveen F Wahid, my major advisor and committee chair, for her guidance and support over my five years at the University of Central Florida. She taught me many things inside and outside of the classroom, and I won't soon forget those lessons.

Dr. Nader Behdad, my co-advisor and committee co-chair, for providing me with a project that turned out to become the basis of my dissertation, and for his support throughout difficult times.

The members of my dissertation committee: Dr. Thomas Wu, Dr. Brian Lail, Dr. Linwood Jones, and Dr. John Shen for all of their valuable insight and suggestions on how to improve the quality of this dissertation, and for making the time to be available for me.

The members of the Antenna, RF, Microwave, and Integrated Systems (ARMI) lab for the abundance of peer support. Particularly, I would like to acknowledge Ajay Subramanian, Mudar Al-Joumayly, Yazid Yusuf, and Justin Luther for their always valuable insights and contributions, and more importantly for their personal friendships. Thank you for making our office a place we loved to be rather than simply "where we worked." I will always look back on those days with sincere fondness.

My family and friends, who have been incredibly supportive of me throughout my academic career. Without all of you, I certainly would not have made it this far. Thank you.

My Wife, Robyn, who is everything to me, for being the one and only constant I can always depend on. Thank you for your love, patience, and sense of humor.

My Mother, Marianne, who has always believed in me, inspired me to do my very best, and encouraged me to always reach higher. Without your love and support I would not be who or where I am today. Thank you.

TABLE OF CONTENTS

LIST OF FIGURES

LIST OF TABLES

LIST OF ACRONYMS/ABBREVIATIONS

3G – Third Generation

ARMI – Antenna, RF, Microwave, and Integrated Systems

BST – Barium Strontium Titanate

CBSA – Cavity Backed Slot Antenna

CP – Circular Polarization

CRLH – Combination Right Left Handed

DBS – Direct Broadcast Satellite

DOA – Direction of Arrival

DFCBSA – Differentially Fed Cavity Backed Slot Antenna

DP – Dual Polarization

EBG – Electronic Bandgap

ESA – Electronically Steerable Array

FEM – Finite Element Method

HSPA – High Speed Packet Access

LHCP – Left Hand Circular Polarization

LTE – Long Term Evolution

MEMS – Microelectromechanical Systems

MIMO – Multiple Input Multiple Output

MMIC – Monolithic Microwave Integrated Circuit

PEC – Perfect Electrical Conductor

PTFE – Polytetrafluoroethylene

RHCP – Right Hand Circular Polarization

SICBSA – Substrate Integrated Cavity Backed Slot Antenna

SIW – Substrate Integrated Waveguide

COTM – Communications On the Move

PCB – Printed Circuit Board

PBG – Photonic Bandgap

WiFi – Wireless Fidelity

WiMAX – Worldwide Interoperability for Microwave Access

CHAPTER 1: INTRODUCTION

1.1 Motivation

The past several decades have seen an ever-growing proliferation of wireless communications systems and increased congestion in the electromagnetic spectrum. With each year, we have borne witness to new technologies thus leading to further crowding of the frequency bands allocated to myriad wireless protocols. Reliable communications systems have been required to develop at the same rapid pace to accommodate the additional demands associated with this growth. Pushing the capabilities of systems beyond what has been achieved so far requires the development of new technologies and techniques, which translates to additional challenges that must be overcome by design engineers. Wideband systems are finding increasingly popular deployment, as the capability to process more data and the demand to do so grows, seemingly without bounds. Topping the list of design challenges are antennas needed to satisfy these requirements. To increase the capacity and/or the reliability of wireless communications systems, new technologies such as receiver diversity (both spatial and polarization) or multiple input multiple output (MIMO) communications have been developed. For the same bandwidth and frequency of operation, using two orthogonal polarizations allows for doubling the transmission capacity. This is commonly utilized in Direct Broadcast Satellite (DBS) services, where different television channels or data streams are broadcasted on the same channel with different polarizations. In other situations two orthogonal polarizations can be used to allow diversity schemes when a channel is found to be performing insufficiently. Moreover, wideband dual-polarized

antennas are frequently used in polarimetric and other radar applications. Therefore, the need for the development of highly reliable low-profile and low cost wideband antennas, with the capability to operate under arbitrary polarization, is now felt more than ever.

To this end, significant work has been performed to develop antennas with these properties. With the current advancements in antenna design and the simultaneous emergence of new materials and processes in recent years, we can also begin to address several of the classical problems which have existed in the area of electronically steerable antenna array (ESA) design. One such challenge is the development of light weight and high performance airborne and spaceborne phased array antennas. The development of new fabrication techniques and use of novel microwave components has lead to a considerable reduction in the overall cost and significant reductions in the overall weight of the arrays. In addition, highly versatile software simulation packages that are now available dramatically reduce the amount of computational power and time required for solutions to large and complex designs.

This dissertation is initially focused on the development of a high performance planar antenna which will be well suited for use in an array. It is widely known that surface waves which may exist in planar arrays lead to resonances that result in scan blindness [1]-[2]. Several methods of reducing surface wave propagation have been investigated including subarraying [3] and use of PBG/EBG structures [4]. Subarraying can lead to other problems including bandwidth reduction, the introduction of grating lobes for small scan angles (which in turn leads to reduction in beam efficiency), axial ratio deterioration for circular-polarized arrays, and other reductions in antenna performance. The use of bandgap structures must be carefully considered. Sufficient

spacing must be maintained between the structure and radiating element to prevent coupling. Furthermore, the spacing must be kept small enough to prevent the unit cell size from becoming large enough to introduce grating lobes. As a result, this method serves to greatly complicate the design procedure. The antenna developed in this dissertation is a surface integrated waveguide cavity backed slot antenna (SICBSA) fed by microstrip lines. This is a new approach, in which the use of a surface integrated waveguide (SIW) cavity will very effectively reduce surface wave propagation. This is accomplished without a decrease in the bandwidth or the performance of the antenna. In addition, a straightforward procedure is used to design the antenna.

1.2 Literature Review

1.2.1 Microstrip Patch Antennas

The current state of the art in the design of wideband dual-polarized antennas seems to be dominated by microstrip antennas. Examples of these include dual-polarized single patches employing various feed configurations [5]-[8], or various dual-polarized stacked patches [9]-[11]. Microstrip antennas are generally narrow-band radiators that are susceptible to surface wave propagation, especially when used in array environments. Aperture coupling has been used to increase the bandwidth of dual-polarized or circular-polarized microstrip antennas, where two orthogonal modes are excited via use of either two off centered slots in the ground plane of the patch [5], [9], or by using a cross slot at the center [6], [10]-[11]. When the orthogonal slots are located off center (Figure 1-1), the structure is asymmetric and the axial ratio deteriorates rapidly off the center frequency, resulting in poor polarization purity

bandwidth. The cross slot coupling mechanism (Figure 1-2) does not have this problem and patch antennas utilizing this technique maintain their polarization bandwidth.

Figure 1-1: Two off-centered aperture coupled feeds

Figure 1-2: Crossed-slot coupled feed

However, to maintain polarization purity the apertures must be fed in a way which prevents cross coupling between the orthogonal apertures. Pozar demonstrated several such feed networks in [6]; however each suffers from associated drawbacks related to the narrowband response of microstrip lines which are used as phase shifting elements. These are necessary due to a bend (reversal) in the microstrip feed directions for proper excitation of the aperture. The optimal feed integrates a series of Wilkinson power dividers to accomplish wideband impedance matching and polarization purity. However, in all cases the aperture size required for sufficient coupling is large enough that the aperture itself is radiating. In turn, these antennas exhibit high backlobe radiation levels

which are undesirable. To reduce this effect, the aperture and feed network can be implemented on a higher dielectric constant material in order to reduce the size; however this also leads to a reduction in the gain bandwidth of the antenna [6]. A variation on the cross aperture coupled feed was shown in [10], where the microstrip lines do not require additional phase compensation. Instead, an air bridge is introduced at the microstrip crossover. This design accomplishes a wideband impedance match and avoids the aforementioned phase deviation, however still suffers from degraded polarization purity due to the use of reactive power splitting. The utilized microstrip tee does not provide good isolation between its output ports. Therefore any mismatch occurring at either feed location can result in a reflection at the other feed location. This causes a disruption in the equal amplitude and phase required to ensure that no net voltage is induced across the orthogonal aperture. In addition to dual aperture coupled feeds, other feeding structures for single and stacked patch designs have been reported. In [7] the two orthogonal modes are excited by combining one aperture coupled microstrip feed with a second "L shaped probe" feed. In this design and other similar variations, wide impedance bandwidths are accomplished by using an air substrate for the radiating patch. Thus, the use of support posts are required rendering the antenna less durable. In addition, since the orthogonal modes are excited using two different feeding structures, the gain and axial ratio response vary significantly over the antenna's operating range. In addition to the problems associated with each of the above feeding mechanisms, stacked patch designs rely on multiple layers of coupling and therefore involve inherently more complex design procedures, where many design variables must be optimized simultaneously in order to achieve an acceptable solution.

Moreover, while these designs offer an improved bandwidth, they are still as susceptible to surface wave propagation in the substrate of the antenna as any other microstrip patch antenna.

1.2.2 Slot Antennas

Slot antennas have also been investigated as candidates for designing wideband, single- or dual-polarized radiators [12]. In particular, cavity-backed slot antennas have also been widely used [13]. Cavity backed slot antennas can be implemented to obtain circular polarization with a hemispherical radiation pattern [14]-[19]. Single (probe) feed designs achieve good polarization purity and maintain compactness; however they remain very narrow band [19]. The use of strip or microstrip line feeds [16]-[17] has also been reported, but these designs have bandwidths of less than 10%. In [14], Lindberg reported a cavity-backed slot antenna with a bandwidth of about 20%. However, the slot length of this design was greater than a wavelength. To increase the antenna bandwidth, a ridged cavity was used in [15]. This antenna demonstrates a bandwidth of 32% but it still remains electrically large with physical dimensions of $0.96\lambda_0$ x $0.96\lambda_0$. Such electrically large structures are not suitable for most modern applications where a compact design is critical. In addition, an electrically large antenna will not be a good choice for use in an array environment as the large electrical dimensions of the structure will inevitably result in large spacing between the array elements and lead to the excitation of grating lobes in phased arrays. The size of cavity backed slot antennas can be reduced to achieve miniaturized cavity and radiator dimension. However, these techniques also lead to a significant reduction in impedance

bandwidth. The use of other aperture shapes such as the T slot [20] or U slot [21] has also been investigated as circular-polarized radiators. However, these structures lack the symmetry required to maintain polarization purity beyond a very narrow band.

1.3 Dissertation Overview

1.3.1 General Overview

In this dissertation, a wideband, dual-polarized, substrate-integrated cavity backed slot antenna (SICBSA) is demonstrated in the X-band. The antenna is fed using two differential ports and is backed by a shallow cavity formed using two rows of closely spaced, electroplated via holes embedded in the printed circuit board (PCB) material that supports the radiator. The cavity serves two main purposes. It reduces the possibility of surface wave propagation and creates a unidirectional radiation pattern. The antenna aperture is composed of two orthogonal wide slots, forming a cross at the center of the cavity. A dual differential feeding scheme is used to feed the crossed-slot and prevent coupling between the orthogonal modes. This enables the SICBSA to maintain a high degree of isolation between the two differential ports over a wide impedance bandwidth. Moreover, the microstrip-fed, wide slot radiator utilized in this design has two distinct but closely spaced resonant frequencies with similar electric field distribution. The separation between these two resonant frequencies can be controlled by judicious choice of the feed locations in order to achieve either a dual-band or a wideband mode of operation. The attained wideband, unidirectional SICBSA provides a high degree of polarization purity over its entire frequency band of operation. This makes the SICBSA widely suitable for a multitude of additional applications requiring

wideband polarization diversity, dual-polarization, or circular polarization in addition to its primary proposed purpose. Examples include mobile radio telephone (3G/HSPA+, 4G/LTE, etc.), broadband wireless protocols utilizing MIMO (WiFi-n, WiMAX, etc.), automotive radars, and commercial communications on the move (COTM). In the following sections, and overview is given for each chapter of this dissertation.

1.3.2 Chapter 2: Dual-Polarized DFCBSA Fundamentals

The wideband dual polarized differentially fed cavity-backed slot antenna (DFCBSA) is introduced. Two types of cavities are presented and compared. In the simplest form a continuous solid metal cavity wall can be used. A modified cavity wall consisting of a series of electroplated vias is introduced in order to facilitate standard fabrication processes as well as to accommodate the use of the antenna in an array. The resulting antenna topology is discussed in detail and the principles of its operation are developed. The dual resonance observed for a wide microstrip fed slot is examined and a means for controlling these resonances is explained. A dual differential feeding scheme is introduced, and the resulting aperture electric field distributions are presented. Finally, the radiation characteristics of the dual polarized DFCBSA are examined. This includes a discussion on the polarization configurations which can be achieved for the DFCBSA. Depending on how the dual-differential feed is configured, vertical polarization, horizontal polarization, dual-polarization, or circular polarization (LHCP or RHCP) may be obtained.

1.3.3 Chapter 3: Design & Simulation

Utilizing the fundamentals developed in Section 2.2, a straightforward design procedure is outlined. A parametric study is carried out to verify the effect of adjusting the feeding locations of the antenna. A dual-polarized substrate integrated waveguide cavity-backed slot antenna (SICBSA) is designed to operate with a center frequency of 10 GHz, average gain of 5.3 dBi, a bandwidth of 19%, an isolation of approximately 30 dB, and hemispherical radiation patterns in each principle plane of the far field. The radiation characteristics are demonstrated to be consistent over the entire wideband operational range of the antenna.

1.3.4 Chapter 4: Fabrication & Measurement

The designed X-band prototype is fabricated as a proof of concept. The fabrication procedure is outlined in order to establish the practical nature of the antenna. The processes used are standard fabrication techniques which are readily available at any PCB fabrication house. The proof of concept prototype was fully characterized at the Antenna, RF, Microwave, and Integrated Systems (ARMI) lab at University of Central Florida. The input reflection for each (polarization) feed, radiations patterns over the entire operational range, and the gain versus frequency are presented and compared with simulation results. The results are analyzed and sources of discrepancy are identified and accounted for in subsequent simulation. Finally, the revised simulation results are demonstrated to be very consistent with the prototype measurement results.

1.3.5 Chapter 5: Use of SICBSA as an Antenna Array Element

The use of the SICBSA as an array element is demonstrated. The unit cell spacing is studied and the effect of mutual coupling on the antenna input impedance and isolation is illustrated. The gain and radiation patterns for a two element linear array are presented and discussed. A uniform two element phased array is demonstrated to scan the main beam from boresight to thirty degrees. Finally, the feed network and phase shifter design is considered and discussed.

CHAPTER 2: DUAL-POLARIZED DFCBSA FUNDAMENTALS

2.1 Basic Topology of the Dual-Polarized DFCBSA

Figure 2-1 presents a perspective view of a wideband dual-polarized differentially fed cavity-backed slot antenna (DFCBSA). The DFBSA is composed of a wide cross-shaped slot situated on top of a dielectric substrate. The bottom side of this substrate is entirely covered with metal. The side walls are also covered with metal and used to complete the cavity. A second, thin dielectric substrate is placed on top of the antenna aperture and four microstrip lines are located on the top surface of this dielectric substrate and are used to feed the antenna. In this configuration the dual-polarized DFCBSA is suitable for practical use as a single radiating antenna. However, if it is desired to use the DFCBSA as the element in an array, continuous metal cavity walls will not be practical for fabrication. For this reason, a slightly different topology may be used where the continuous cavity is replaced by a substrate integrated waveguide (SIW) cavity as shown in Figure 2-2. In this configuration, two rows of closely spaced vias are used to form the cavity side walls. The antenna operation remains the same in other regards, and the only effect of changing the type of cavity used is a slight difference in the required dimensions of the antenna for operation in a particular frequency range and to impedance match the antenna to its feeding transmission lines.

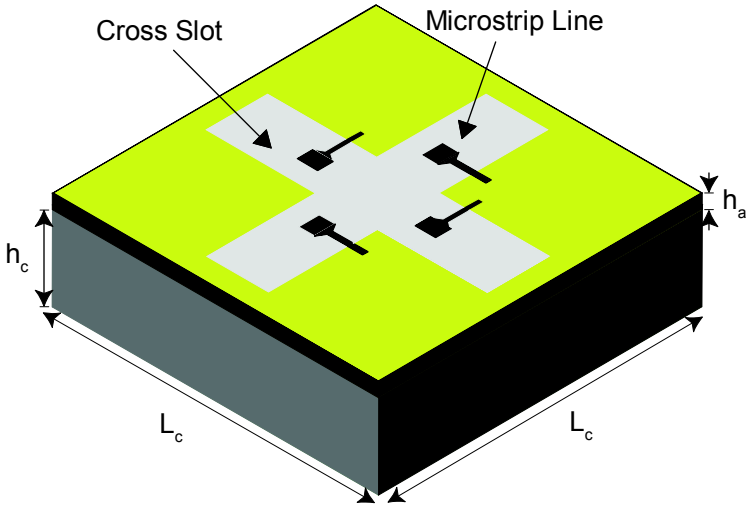

Figure 2-1: Perspective view of the continuous cavity DFCBSA

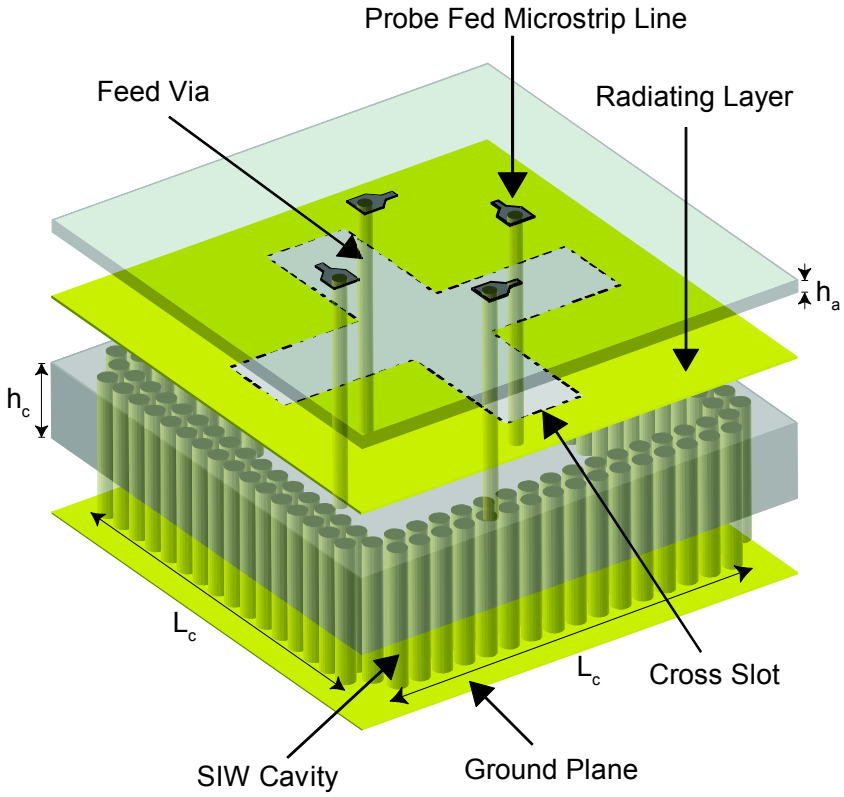

Figure 2-2: Perspective view of the SICBSA

Detailed views of the antenna stack up and the relative locations of the feeding elements with respect to the radiating elements are shown in Figure 2-3 and Figure 2-4. In these figures, a SIW cavity is illustrated. The four microstrip line feeds are connected to four feeding coaxial cables located beneath the cavity using four vias that extend from the feed layer on the top to the bottom of the cavity, where they are connected to the center conductors of their respective cable. The outer conductors of the coaxial cables are connected to the bottom wall of the cavity.

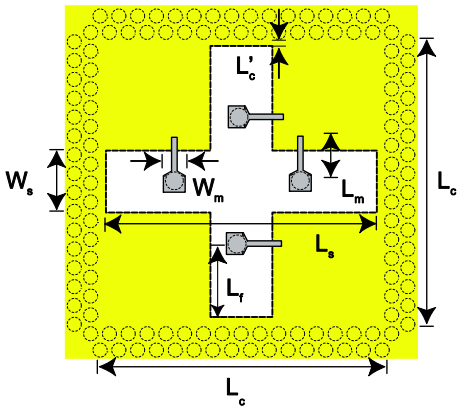

Figure 2-3: Top view of the SICBSA

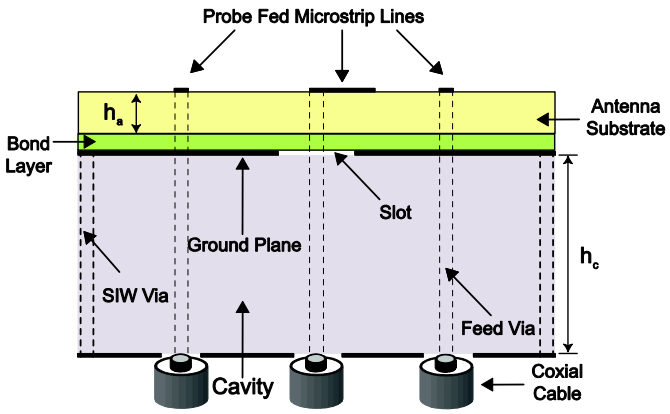

Figure 2-4: Side view of the SICBSA

It is also possible to use a different feeding arrangement in which the microstrip lines are placed below the slot layer. This design will have the advantage of isolating the feeding structure from the outside world. Moreover, in this topology, the antenna aperture will not be covered with a dielectric substrate that can support surface waves. However, to demonstrate a proof of concept the former topology is adopted mainly in order to facilitate the possibility of physically tuning the feeding network of the prototype (this is discussed in Section 4.2). The substrate integrated waveguide (SIW) cavity is

formed by connecting the ground plane, which contains the cross slot, to the bottom of the antenna using two rows of closely spaced vias. This also serves to form a common ground between the cables and the microstrip line feeds.

2.2 Mode Of Operation

In [22], Behdad showed that a wide radiating slot can demonstrate a double-resonant behavior when it is fed with an off center microstrip line. The second resonance is caused by a fictitious short circuit created by that portion of the microstrip line without any ground plane. Thus, by changing the location of the microstrip line, the frequencies of the two resonances can be adjusted and either a wideband or a dual-band response can be obtained. The use of an open circuited microstrip stub also provides a degree of flexibility in matching the input impedance of the antenna to that of its feeding transmission line. It is desired to extend this dual-resonant behavior to the present dual-polarized SICBSA. However, the crossed slot structure can support several additional resonant modes which would not arise for a simple rectangular slot antenna. Namely, by exciting either slot with one microstrip, a net voltage will be induced across both slots. Therefore, it may be possible that both slots radiate when only one is fed. This will translate to a high level of cross polarized radiation and a low level of isolation between the two slots' feeds. Therefore, to ensure that the antenna is fed in a balanced fashion and undesired modes are not excited, a differential feeding scheme is employed, whereby each slot is fed on either end of the cross junction with equal amplitude and 180˚ phase difference. The resulting aperture electric field distributions are similar to those shown in Figure 2-5 and Figure 2-6, which were

obtained using full-wave EM simulations conducted in CST Microwave Studio. Figure 2-5 shows the aperture electric field distribution at the first resonance, when the antenna is differentially excited at ports 1 and 3, with ports 2 and 4 terminated in matched loads.

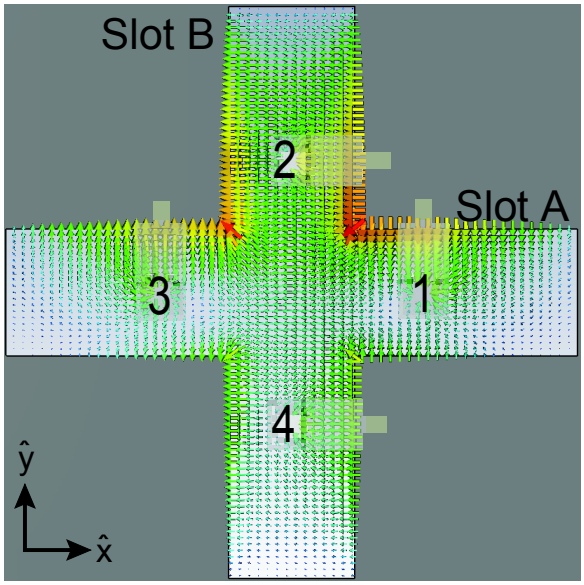

Figure 2-5: Aperture electric field distribution at first resonance

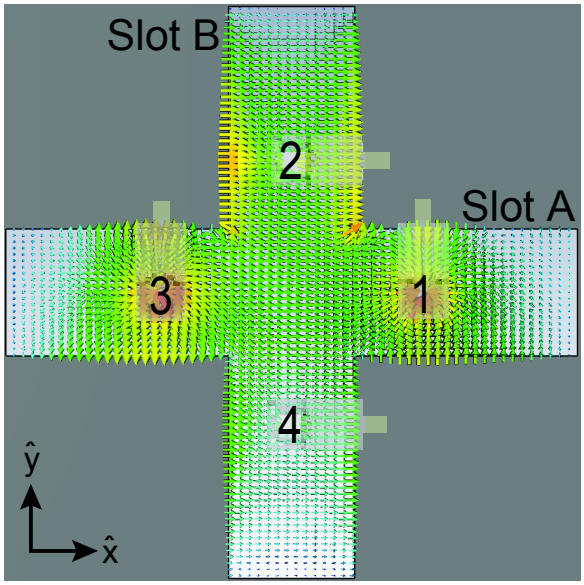

Figure 2-6: Aperture electric field distribution at second resonance

As a result of the 180˚ phase difference between ports 1 and 3, the electric field distribution is anti-symmetric along slot A and hence this slot does not significantly contribute to the far-field radiation. However, the field distribution along slot B is symmetric and resembles that of a half wavelength slot. Therefore, when ports 1 and 3 are differentially excited, the effective magnetic current over the aperture would be directed along the $\hat{y}$ direction. As a result, the far-field radiation would be horizontally polarized (directed along the $\hat{x}$ direction at boresight). On the other hand, if ports 2 and

4 are differentially excited, with ports 1 and 3 matched, slot B will have an anti-symmetric field distribution and the radiation in the far field will mainly come from slot A. In this case the radiated field will be vertically polarized in the far-field ($\hat{y}$ direction). This mode of operation is different from the one presented in [22], since in the present case, the slot which is directly fed (resonant) is not the main radiator. It can be seen that a half sinusoidal distribution is observed across the length of the radiating slot.

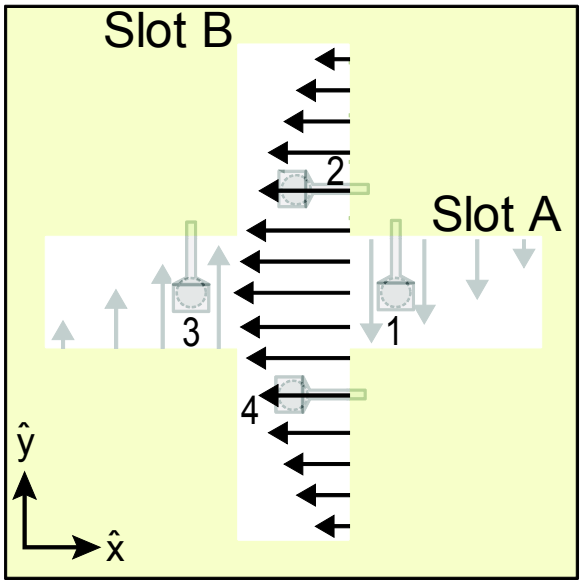

Figure 2-7: Illustrated aperture electric field distribution at first resonance

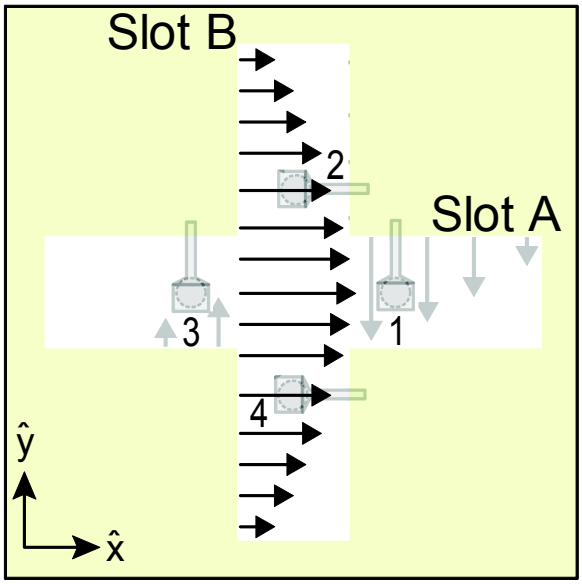

Figure 2-8: Illustrated aperture electric field distribution at second resonance

In order to maintain reliable performance the excited aperture field distribution should be consistent over the entire operating range of the antenna. The electric field distribution over the aperture, at the second resonance, is shown in Figure 2-6. It can be seen that the electric field distribution along slot A again exhibits anti-symmetry, albeit with a slightly shorter resonant length (corresponding to the higher resonant frequency). The

excited field distribution along the radiating slot is indeed seen to be consistent over the operating frequency range, indicating that a uniform radiation characteristic can be expected over a wide bandwidth.

To clearly illustrate this mode of operation, the aperture electric field distributions at the first and second resonances are also portrayed in Figure 2-7 and Figure 2-8. The distributions shown here qualitatively illustrate what is seen in Figure 2-5 and Figure 2-6.

Quadrature feeding may be employed to achieve circular polarization, resulting in feeding the 4 ports of the antenna with equal amplitudes and phases of 0˚, 90˚, 180˚, and 270˚. This way, the two orthogonal apertures can be excited with the desired modes and a phase separation of 90˚.

CHAPTER 3: DESIGN & SIMULATION

3.1 DFCBSA Design Procedure

As established in Section 1.2, one of the main advantages of the wideband dual-polarized SICBSA is the ease of design. The primary parameters that affect the performance and frequency response of the antenna are the location of the microstrip feed lines, L_f, the length of the open circuited microstrip stubs, L_m, and the width of the radiating slots, W_s. The slot length, L_s, and the feed locations, L_f, are the two main parameters that determine the resonant frequencies of the antenna. The length and width of each slot and the dimensions of the four microstrip line feeds are all kept identical to preserve the symmetry required for wideband polarization purity. L_s mainly affects the center frequency of operation of the antenna and L_f determines the separation between the two resonant frequencies. A study on the effect of adjusting the feed locations, L_f, on the resonant frequencies of the antenna is conducted and the results are presented in Figure 3-1. In this study, a continuous cavity DFCBSA (similar to the one shown in Figure 2-1) is used in order to reduce the simulation time required to complete many design iterations. It is desired to display as large a tuning range for the feed locations as possible. Therefore, the coaxial cables used to connect the feeding vias are replaced with ideal gap (lumped port) sources located just between the cavity bottom and each feed via. This allows for placing the feeds closer to each other. However, the ideal response of a lumped 50Ω source presents no additional loading to the input impedance of the antenna. Therefore, the results presented in Figure 3-1 may differ slightly from an antenna fed with actual coaxial cables but irrespective of the feed

type, the same general trend will be observed. The structure is analyzed using full-wave EM simulations in CST Microwave Studio and the antenna is optimized to provide a good impedance match at both resonant frequencies. It is observed that as L_f increases, the separation between the two resonant frequencies becomes larger. This is due to shortening the resonant length of the second mode and increasing the loading effect of the microstrip feeds at the first mode. Once the two resonances are obtained at the desired frequencies, the antenna is impedance matched by tuning the length of the open circuited microstrip stubs, L_m.

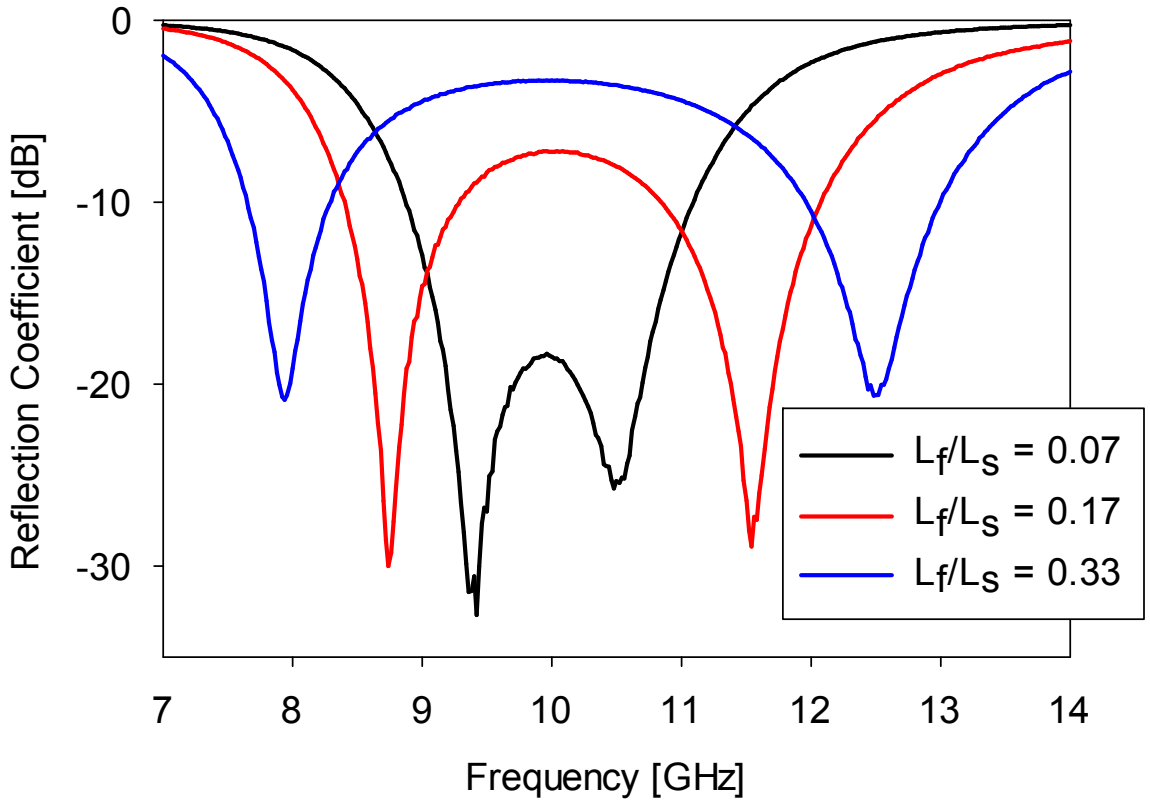

Figure 3-1: Effect of Feed Location

The reactive impedance introduced by the stub will compensate the reactive part of the input impedance of the antenna. It is evident that either a wideband or a dual-band response can be obtained simply by adjusting the feeding location (L_f). As mentioned above, the width of the slot, W_s, also has a significant effect on the performance of the antenna. The slot width primarily affects the bandwidth of the individual resonances. Furthermore, if too small a slot width is used, the second resonance may not be visible. Likewise, too large a slot width will lead to degraded impedance matching and other effects. A more in depth discussion on the variation of the dimensions of offset microstrip fed wide slots is given in [22]. The final parameter which has a strong effect on the antenna (and all cavity-backed slot antennas) performance is the size of the cavity, L_c. Although this is primarily determined by the length of the slot, the exact spacing between the slot edge and cavity edge (L_c' as shown in Figure 2-3) can be varied slightly to optimize impedance matching. In general the cavity size should be roughly the same size (slightly larger) than the slot length.

3.2 Design of A Differentially Fed SICBSA at X-Band

3.2.1 General Considerations

A prototype antenna similar to the one shown in Figure 2-2 is designed to operate in the X-band. In order to achieve a wide bandwidth and high radiation efficiency, a low dielectric constant, low loss ($\varepsilon_r = 2.2,\ \tan\delta = 0.0009$) substrate, Rogers RT/duroid® 5880, is chosen for the cavity and the antenna substrate. This composite material is manufactured from polytetrafluoroethylene (PTFE), a

fluorocarbon-based polymer. In order to maintain consistent electrical properties in the adhesion layer, a thermoplastic chloro-fluorocopolymer based bond material, Rogers 3001, is selected due to its similar dielectric constant and low loss ($\varepsilon_r = 2.28,\ \tan\delta = 0.003$). A cavity substrate thickness of 3.175mm is selected from amongst the standard values available from the manufacturer, resulting in a cavity height of approximately $\lambda_0/11$. The top antenna substrate is chosen to be 0.508 mm as a balance between practical microstrip dimensions (to minimize the effect of fabrication tolerances) and total antenna profile. The bonding layer standard thickness is 0.381mm, resulting in a total antenna stackup height of $0.12\lambda_0$.

3.2.2 Fabrication Considerations

Close attention must be paid to the method by which the SIW cavity is formed to facilitate fabrication and provide accurate measurement results. Highly standardized fabrication processes need to be used which also lead to reduced cost since only streamlined manufacturing techniques need be used to fabricate the antenna. The SIW cavity formation is discussed in detail in Section 4.1. The two basic considerations for the SIW cavity design are the diameter of the vias and the spacing between adjacent vias. These dimensions must be chosen such that two criteria are met simultaneously. The vias must effectively act as a continuous cavity wall (i.e. the tangential electric field is zero), and the dimensions must be practically achievable using a standard fabrication process. In [23] the conditions to prevent “radiation leakage” are established in terms of the via diameter, D, and the via spacing, b. These conditions are summarized in

Equations (3-1) and (3-2), where λ_g is the guided wavelength inside a substrate integrated waveguide.

$$D < \frac{\lambda_g}{5} \quad \textbf{(3-1)}$$

$$b < 2D \quad \textbf{(3-2)}$$

In the present case the SIW is used not as a guiding structure, but as a cavity. Therefore it is not straightforward to calculate λ_g, however Equation (3-1) puts a practical upper limit on the via diameter. If the spacing is kept much smaller, the same effect can be expected. For a center frequency of 10 GHz, $\lambda_0 = 30\ \mathrm{mm}$. A diameter of $0.7mm$ (approximately $\lambda_0/43$) is chosen for the design so that a standard drill bit can be used. It can be reasonably assumed that this value is sufficiently small to meet the above criteria. The vias are spaced apart by $0.23\ mm$ (roughly $\lambda_0/130$, $\mathrm{b} = 0.33\mathrm{D}$). This value is determined by the diameter of the vias, the number of vias used, and the size of the cavity. Then the criteria of Equations (3-1) and (3-2) are met and fall well within the PCB manufacturer's specified tolerance of $150\ um$ resolution. In order to accommodate the possibility of potential fabrication errors during the plating process, two rows of metal vias are used to form the cavity wall. Therefore in the event that some vias are not properly plated, the second row of vias will serve to provide the proper boundary.

3.2.3 Modeling Considerations

Ansoft HFSS, a commercial full wave electromagnetics software package is used to design the SICBSA. The finite element method (FEM) solver performs a full three dimensional adaptive meshing of the structure to accurately capture the changing fields. The size of the mesh can significantly impact the simulation time required for accurate results. The SIW cavity vias are formed by drilling holes and depositing a layer of copper inside, resulting in a large number of hollow (air filled) metal cylinders around the edges of the antenna. Including these hollow copper cylinders in the HFSS model won't result in significantly increased accuracy as compared with the substitution of solid perfect electrical conducting (PEC) cylinders. The resulting design is shown in Figure 3-2 and will be accurate (provide good measurement results) as long as the deposited metal thickness of the fabricated prototype is at least several times the skin depth (about $0.65\ \mu m$ for copper at 10 GHz).

The SICBSA and feeding coaxial feeding cables are placed inside of a volume of air which extends a quarter wavelength in each direction from the edge of antenna, as shown in Figure 3-3. A radiation boundary condition is used at the edges of the containing volume of air. This is a second order boundary condition which results in the majority of the incident energy being absorbed (and hence not being reflected back into the simulation space), thereby emulating the effect of the structure being placed in an infinitely large volume (to ensure high simulation accuracy).

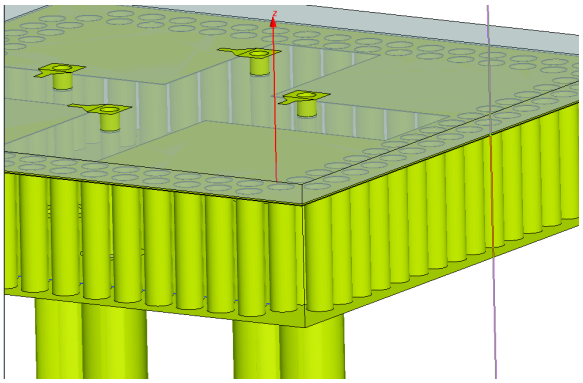

Figure 3-2: SIW cavity vias modeled as solid PEC cylinders in HFSS

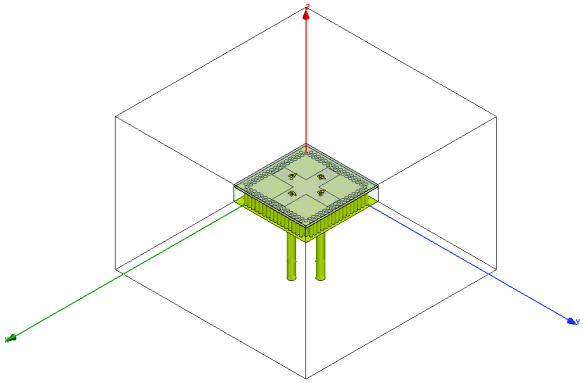

Figure 3-3: SICBSA modeled in a containing radiation boundary in HFSS

The simulated four-port S-parameters are exported from HFSS and further processed with Agilent's Advanced Design System (ADS) software to introduce the required 180° phase differences needed for the proposed differential feeding scheme. The optimized dimensions of the X-band prototype are presented in Table 3-1, and the differential feeding configuration is illustrated in Figure 3-4.

Table 3-1: Optimized dimensions

Parameter	Value (mm)
L_s	14.0
W_s	3.1
L'_c	0.1
L_f	3.5
L_m	0
h_c	3.175
h_a	0.508

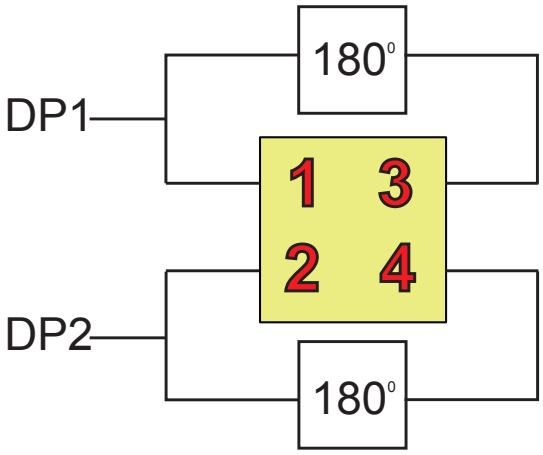

Figure 3-4: Differential feed block

The four antenna feeds are defined in the same manner as depicted in Figure 2-5. Differential port 1 (DP1) is obtained by feeding ports 1 and 3 with the same magnitude and 180˚ phase shift. Similarly, differential port 2 (DP2) is obtained by feeding ports 2 and 4 with the same magnitude and 180˚ phase shift. In this configuration, DP1 and DP2 form the two inputs which determine the polarization of the antenna. For example, if DP1 and DP2 are fed with equal power and quadrature phase, the resulting radiation will be circularly polarized. Alternatively, DP1 and DP2 may be fed with two distinct signals and an effective doubling of bandwidth is obtained as the antenna radiates in a dual linearly polarized mode.

3.2.4 X-Band SICBSA Simulation Results

The simulated input reflection coefficient for each differential port and isolation between the two differential ports are shown in Figure 3-5. It can be seen that each differential port achieves a 19% impedance bandwidth ($D-S_{11}<-10\,dB,\ D-S_{22}<-10\,dB$). In addition, the isolation between the two differential ports ($D-S_{21}$) is better than $30\,dB$ across the operational range of the SICBSA. These results are compared with measured results in Section 4.2. The simulated radiation patterns in each principle plane are shown in Figure 3-6 and Figure 3-7. The radiation patterns are shown near the center of the operating range of the prototype design. It can be seen that hemispherical patterns are obtained in the E-plane and the H-plane of the antenna. A gain of about $5.6\,dBi$ is achieved, with a low level of cross-polarized radiation (approximately $25\,dB$ down). The radiation patterns are very similar over the entire operating range of the antenna, as will be demonstrated in Section 4.5.

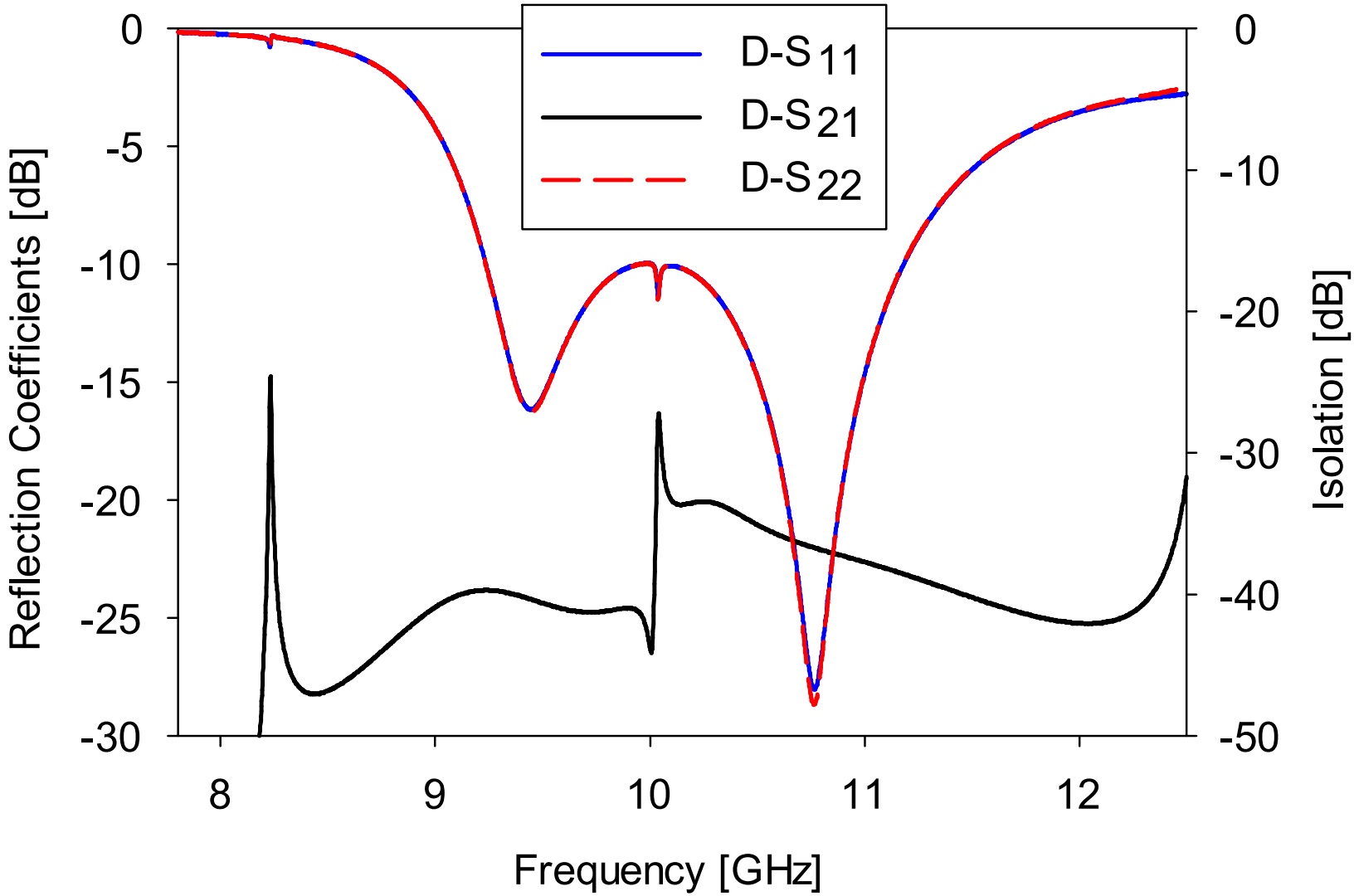

Figure 3-5: Simulated s-parameters

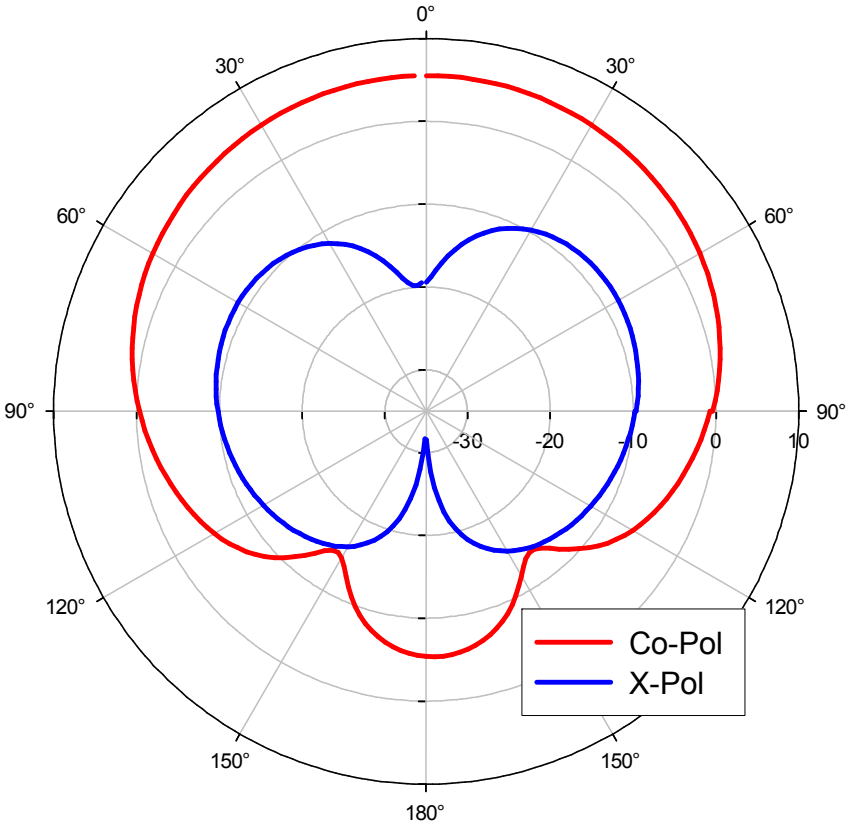

Figure 3-6: Simulated E-plane radiation pattern at 9.5 GHz

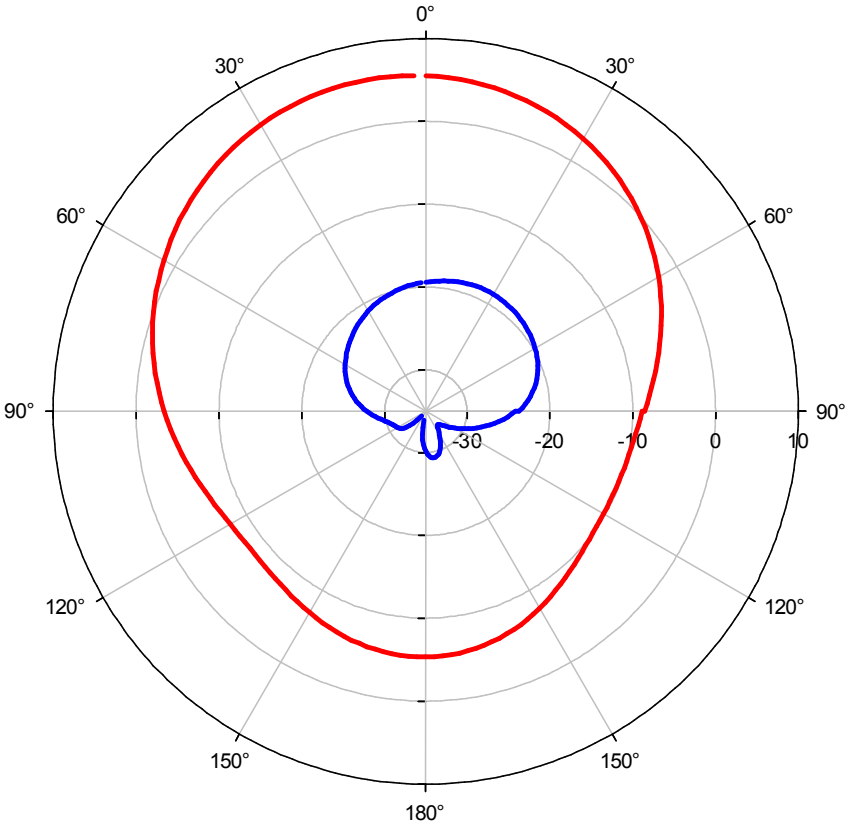

Figure 3-7: Simulated H-plane radiation pattern at 9.5 GHz

CHAPTER 4: FABRICATION & MEASUREMENT

4.1 Fabrication of a SICBSA Proof of Concept Prototype

To validate the predicted performance of the designed SICBSA, a prototype antenna is fabricated. An initial fabrication was carried out at the Antenna, RF, Microwave, and Integrated Systems (ARMI) lab at the University of Central Florida. The prototype was created using an LPKF ProtoMat S100 rapid prototyping system, UV photolithography, visual alignment of the top and bottom substrate, and simple soldering to bond the layers together. It was determined that the obtained alignment accuracy was not sufficient for consistent measurement results. Therefore, a commercial PCB fabrication service was utilized for the fabricating the prototype. The microstrip line feeds and the crossed slot are fabricated using standard UV photolithography. The microstrip feeds are patterned on a 20 mil thick Rogers RT/duroid 5880® substrate. To create the cavity, the crossed slot is etched out of one side of a double sided copper plated 125 mil thick RT/duroid® 5880 substrate. Two layers of holes are drilled around the edges and are metalized to form the SIW cavity walls. The modeled SICBSA prototype maintains its performance when only one layer of vias is used; however, two rows are used in the prototype to account for the possibility of fabrication errors. As mentioned previously, the duroid substrate is manufactured from a PTFE polymer. Therefore, to achieve good adhesion in the electroless (copper) metallization process, a sodium treatment is used to prepare the surface prior to the deposition. Similarly, an alternative oxide process is applied to the ground plane on top of the cavity (which contains the crossed slot). The copper is treated in order to promote good adhesion with

the bottom PTFE surface of the top antenna substrate. The antenna substrate is placed on top of the cavity, aligned with respect to the cavity walls, and bonded together using Rogers 3001 bonding film. Finally, holes are drilled through the entire assembly at the four feed locations. The final process of assembling the feeds was done at University of Central Florida. The coaxial cable feeds' center conductors are inserted through the bottom holes, extended through SICBSA, and connected to the microstrip lines on the top. The outer conductors of the coaxial cables are connected to the cavity bottom. Care is taken to ensure that the length of each of the four coaxial cables is the same. This is important in order to ensure that the antenna is fed differentially with a phase shift of 180˚ between ports 1 and 3 or ports 2 and 4. The assembled antenna is shown in Figure 4-1.

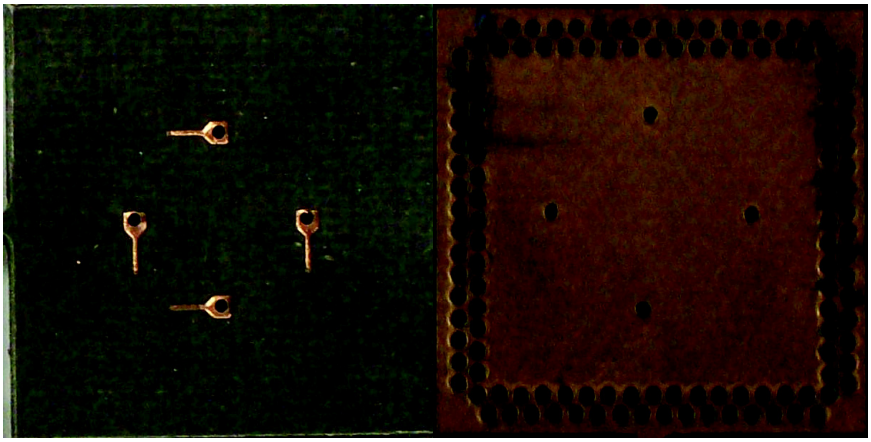

Figure 4-1: X-band proof-of-concept prototype

4.2 S-Parameter Measurements for the SICBSA Prototype

The S parameters of the fabricated antenna are measured using an Agilent N5230A two-port Vector Network Analyzer. Each two port combination is measured with the remaining ports are terminated with matched loads. The required 180˚ phase shifts are then added in a post processing step in ADS. The measured input reflection coefficients for each differential port and the isolation between the two differential ports are plotted in

Figure 4-2. It is observed that the same 19% impedance bandwidth predicted by the simulations of Section 3.2.4 is obtained for both DP1 and DP2 (D-S_{11} < -10 dB, D-S_{22} < -10 dB). In addition, the isolation between the two differential ports is maintained close to the predicted 30 dB level.

The discrepancy observed between the measurement and simulation results can be attributed to two main sources: fabrication issues and measurement errors. The fabricated antenna structure is not identical to the one which was simulated. In simulations, each small dimension can be precisely controlled, whereas in the prototype fabrication, there are tolerances that can cause variations of the actual physical and electrical parameters of the structure from the desired ones. More specifically the fabrication issues discussed below have contributed to the differences observed between the simulation and measurement results.

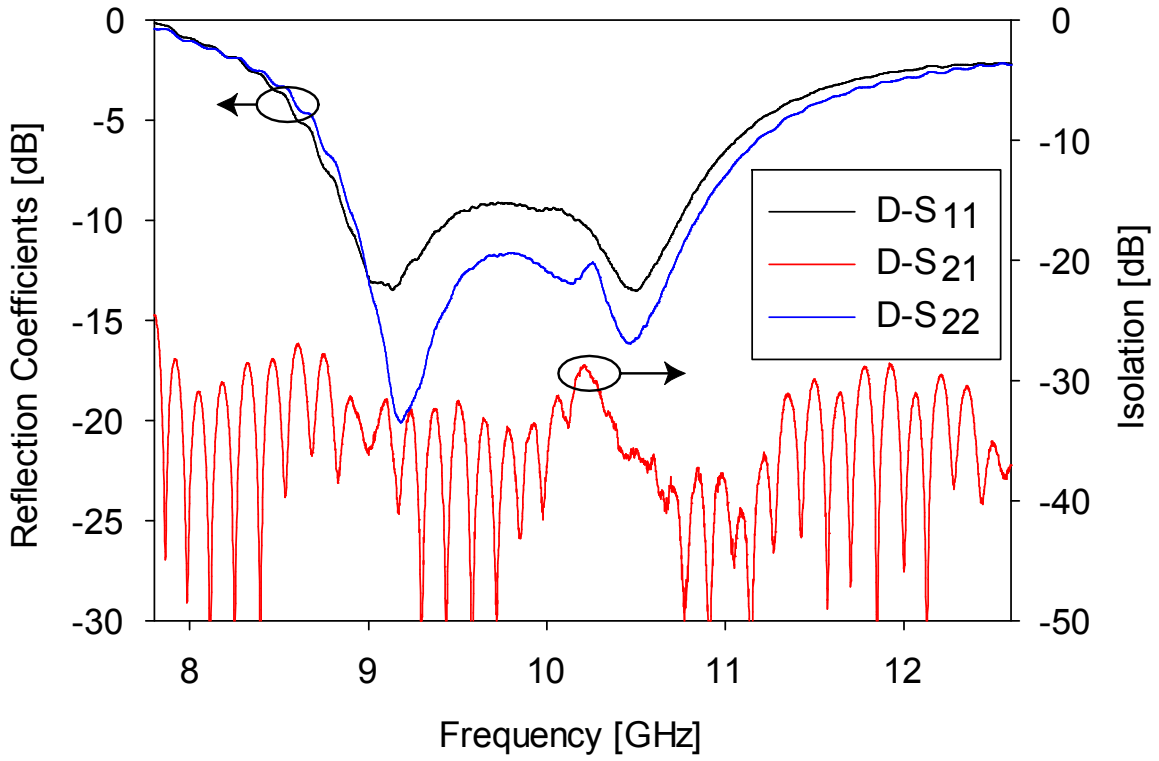

Figure 4-2: Measured s-parameters

4.3 Possible Sources of Discrepancy between Simulated and Measured Results

There is a ±5% uncertainty in the exact values of the dielectric constant and loss tangent of the materials used to fabricate the antenna. The lithography process used by the fabrication service has a resolution of 0.15mm. As specified by the service provider, the PCB shop could guarantee the dimensions of the structure only to within ±0.15mm. The antenna is composed of three different metal layers which need to be aligned perfectly with respect to one another. In particular, the microstrip feed layer on top and the cross slot layer in the middle layer should be perfectly aligned with respect to one another, and with respect to the location of the center of cavity. However, this is limited by the fabrication process used. In this particular fabrication process, the alignment

accuracy was ±0.15mm. These fabrication tolerances do not significantly affect the performance of low frequency antennas. However, as frequency increases, these small variations become more important as the physical dimensions of antenna decrease.

Additional fabrication issues arise from factors introduced by the assembly of the feeding lines. The antenna is fed using four coaxial cables which are soldered into place at the bottom of the cavity. The cables are cut into appropriate lengths by hand and manually assembled. Therefore, small variations in the lengths of these cables are to be expected. Furthermore, In order to prevent the short circuiting of the feed vias to the cavity bottom, a small area of copper is removed around the contact point where the feed via and center conductor of the cable are connected. This area is created using a small diameter milling bit and a hand operated drill press. Small variations in the size of the area removed for each port as well as the relative angling of the soldered cable will lead to a minor variation in the input impedance for the corresponding port. Moreover, the length of the open circuited microstrip line stub used to impedance match each port is manually adjusted by means of removing incremental lengths of the copper. The inherent tolerance of adjusting each line uniformly leads to an additional variation between each port's input impedance.

In addition to the above mentioned fabrication sources of errors, certain measurement inaccuracies can contribute to the observed discrepancies between the measured and simulated results. One of the main sources of measurement errors is the presence of two coaxial cables in the vicinity of the antenna during the S-parameter measurement. These feeding cables have relatively large dimensions compared to those of the antenna and are located in its near field. In spite of these fabrication and

measurement issues, a relatively good agreement between the measured and simulated results is observed. A dual resonance centered near 10 GHz is observed, as expected. In addition, there is a high degree of isolation between the two differential ports over the entire matched bandwidth.

4.4 Modeling Fabrication Issues

Recognizing the sources of discrepancy between the simulated and measured results, an attempt was made to arrive at a modified antenna model which includes small variations from the earlier model. The parameters varied are the length and width of the printed crossed slot, a small variation in the overall feeding locations, an asymmetry with respect to the feeding locations of one differential port versus the other, and an asymmetry with respect to the lengths of the open circuited microstrip line stubs of one differential port versus the other. The result of each of these modifications can be summarized as follows. When the overall locations of the feed vias are adjusted, the resonant frequencies are shifted. Similarly, an asymmetry in the feed via locations results in an asymmetry between the resonant frequencies of the two differential ports. A variation in the degree of matching in each differential port is observed with small variations in the lengths of the four microstrip line stubs.

A best attempt to closely model the primary discrepancies observed between the ideal SICBSA simulation and the prototype measurement is shown in Figure 4-3. Due to the practical limitation of simulating a very large number of variations to closely duplicate the observed discrepancies, and the simulation time required for the SICBSA,

the modified simulations are performed using the continuous cavity DFCBSA. The modifications of the dimensions are summarized in Table 4-1.

Table 4-1: Comparison of Orginal and Modified Dimensions

Parameter	Initial (mm)	Final (mm)
L_s	14.0	14.955
W_s	3.1	3.4
L_m	0	0.1
L_f Asymmetry	-	0.45
L_m Asymmetry	-	0.1

Referring to Figure 4-3, the simulated operating frequency range is now matched to the measured results. The simulated asymmetry between the degrees of matching in each differential port also better reflect the measured results. The remaining differences may be attributed to the other variations which are practically impossible to model.

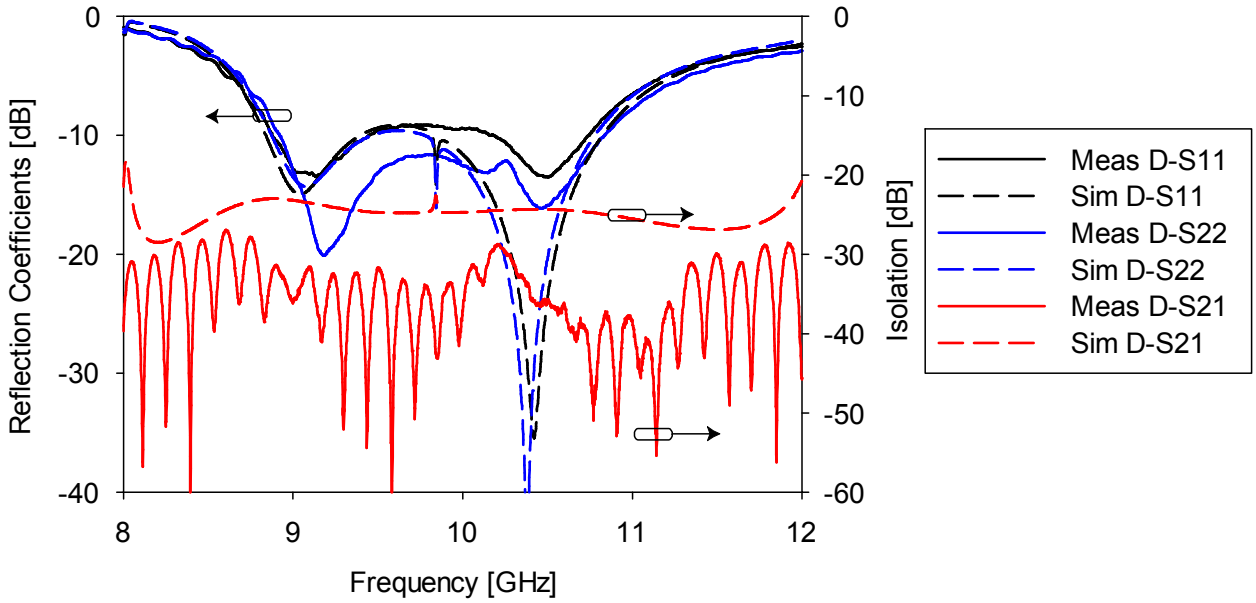

Figure 4-3: Measured and simulated (modified) s-parameters

4.5 Radiation Measurements for the SICBSA Prototype

To achieve the required differential feeding for radiation measurements, a series of 3 dB Wilkinson power dividers are designed and fabricated. As shown in Figure 4-4, one of the output ports of each power divider contains a meandered microstrip line to introduce the 180˚ phase difference required. Due to the narrow band phase response of this circuit, power dividers are designed at each resonant frequency and at an additional frequency between the two resonances. The measurements are performed individually for each frequency using the corresponding power divider. The two output ports of the power divider are connected to one differential port pair of the SICBSA using a short length of coaxial cable. The remaining differential port pair is terminated in matched loads. Care is taken to reduce the effects of the presence of the coaxial cables protruding from the bottom of the fabricated prototype and the power divider circuit in

the pattern measurement. The assembly containing the power dividing circuit, connecting cables, and the antenna feeding cables, are placed inside a fixture covered with microwave absorbing material. The radiation parameters of the antenna including its radiation patterns, gain, and radiation efficiency are measured in the anechoic chamber of the University of Central Florida. The measured radiation patterns are plotted in Figure 4-5- Figure 4-10.

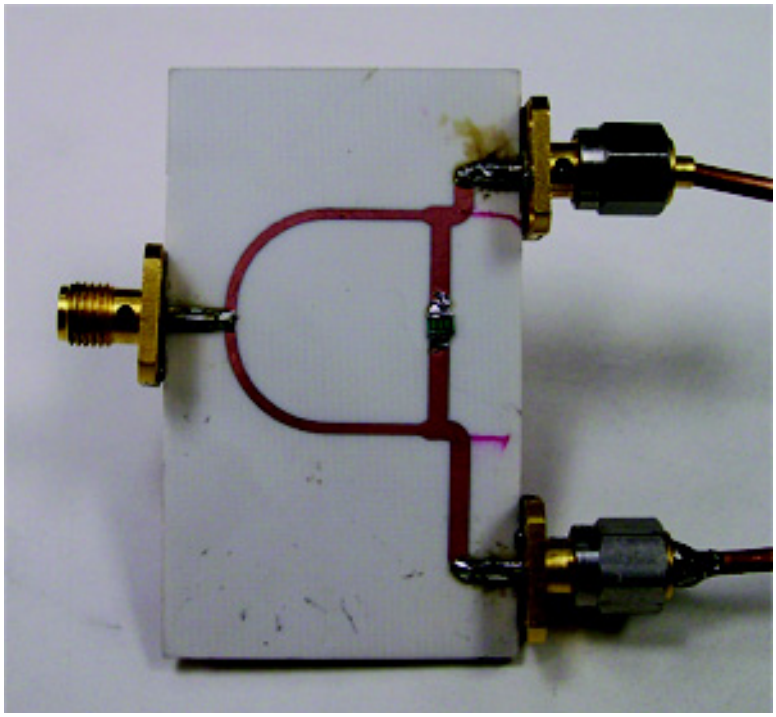

Figure 4-4: Wilkinson power divider with one meandered microstrip line output

It can be seen in Figure 4-5 and Figure 4-6 that a hemispherical radiation pattern is obtained in each principle plane of the antenna at the first resonant frequency. In addition, a very low level of cross-polarized radiation is observed (about -20 dB in the E-Plane and about -25 dB in the H-Plane). The far-field patterns are also presented at the

center frequency and second resonant frequency, 9.5 GHz and 10.47 GHz respectively, in order to illustrate that the radiation characteristics are consistent across the wide operational range of the antenna.

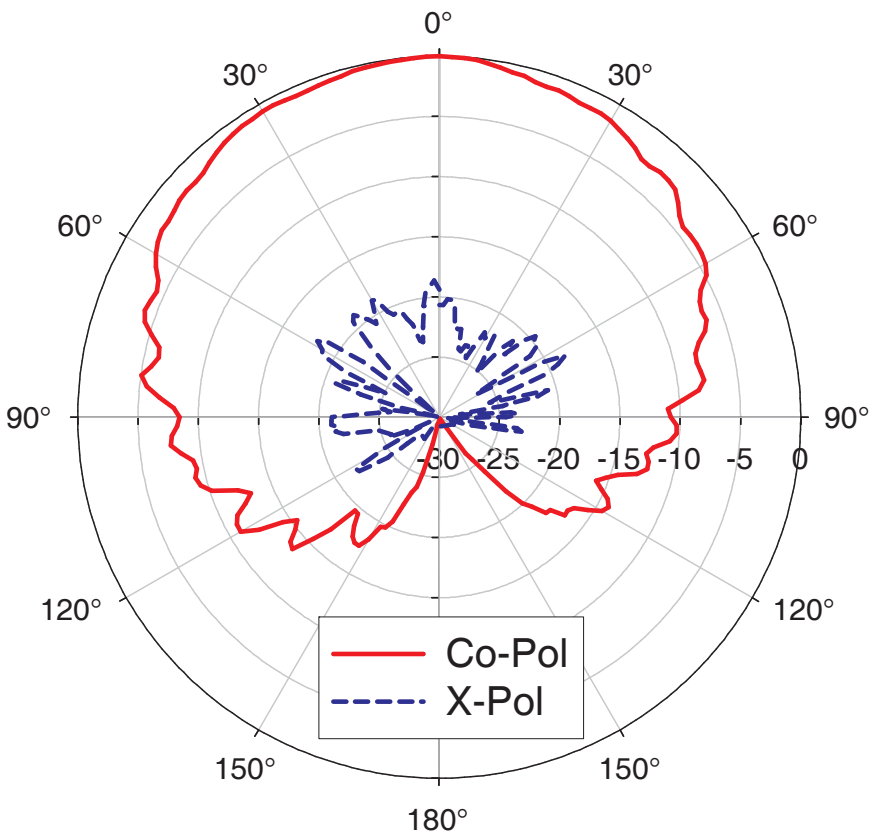

Figure 4-5: Measured E-plane radiation pattern at 9.18 GHz

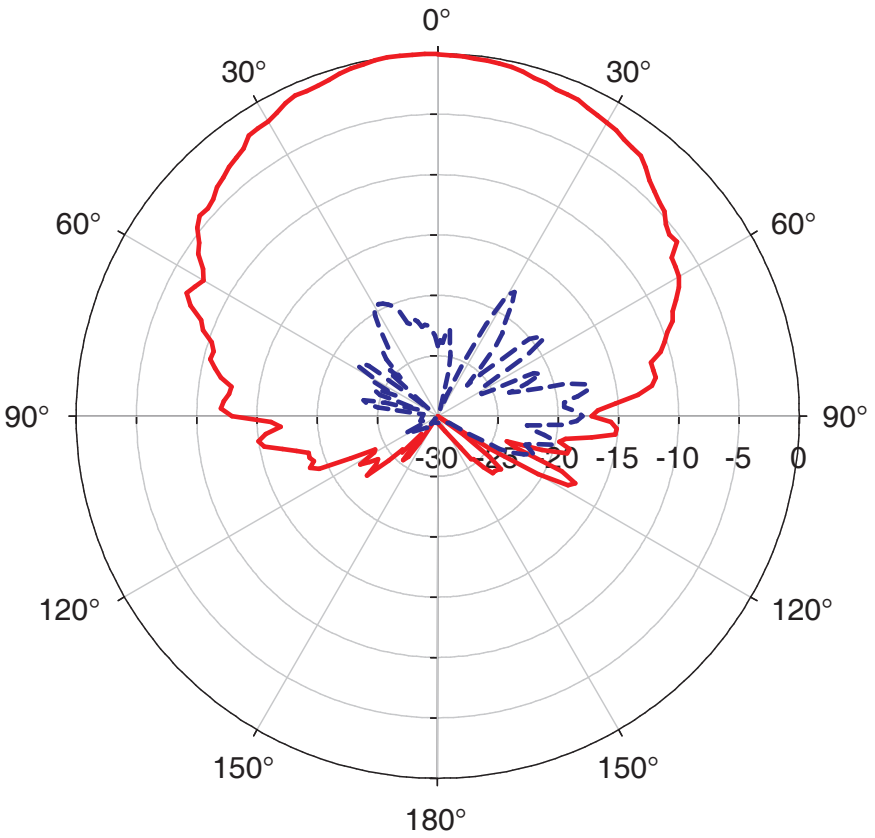

Figure 4-6: Measured H-plane radiation pattern at 9.18 GHz

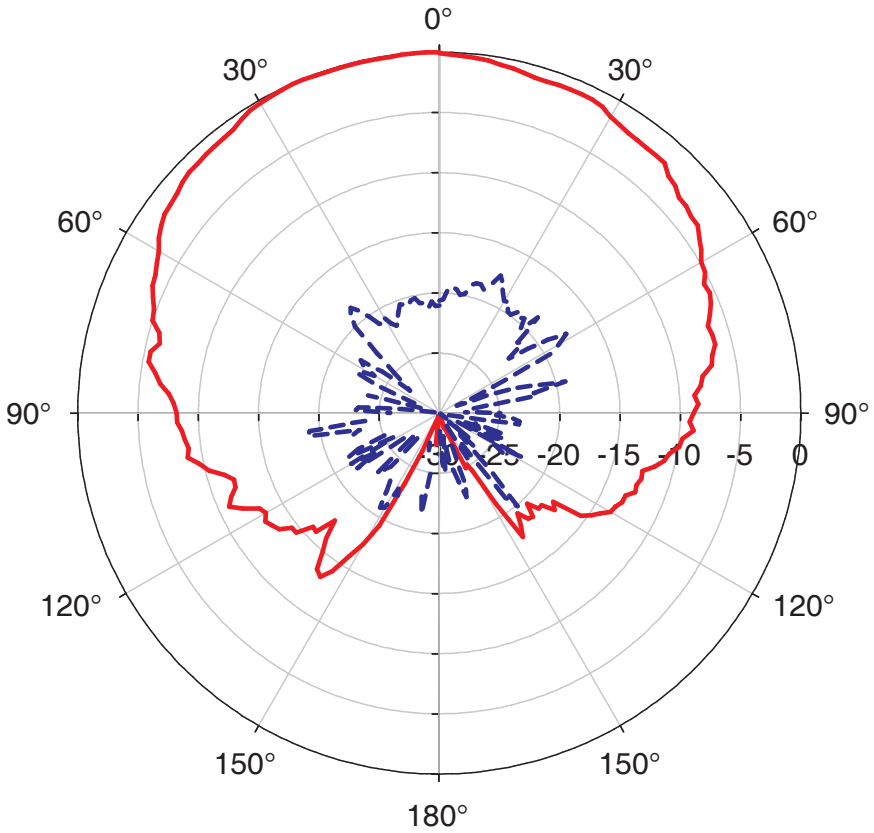

Figure 4-7: Measured E-plane radiation pattern at 9.5 GHz

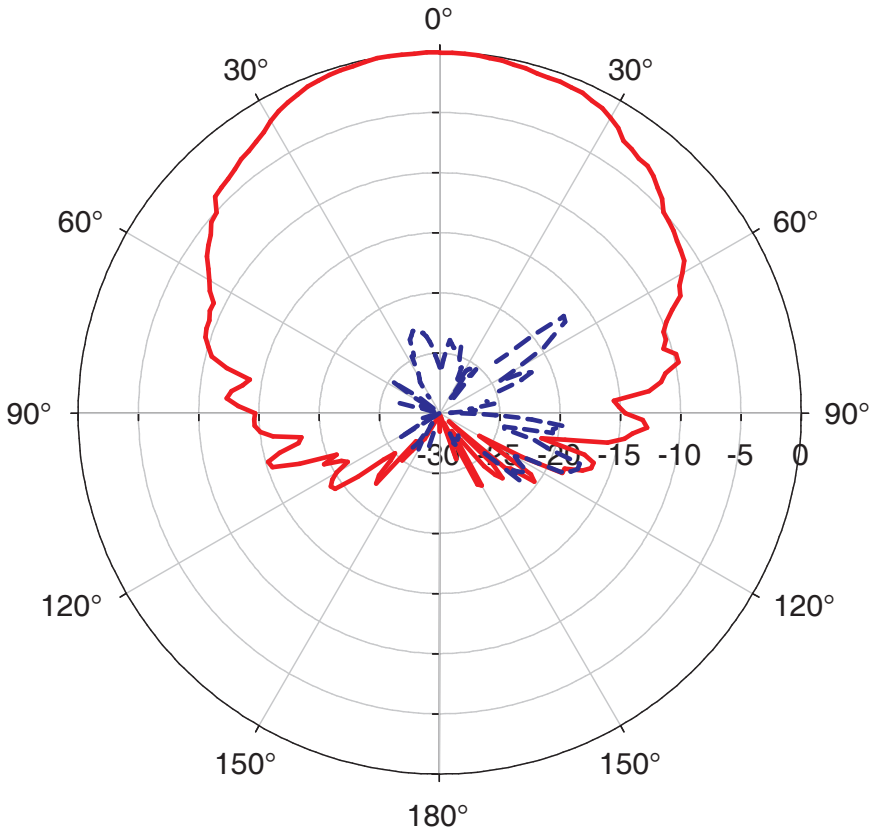

Figure 4-8: Measured H-plane radiation Pattern at 9.5 GHz

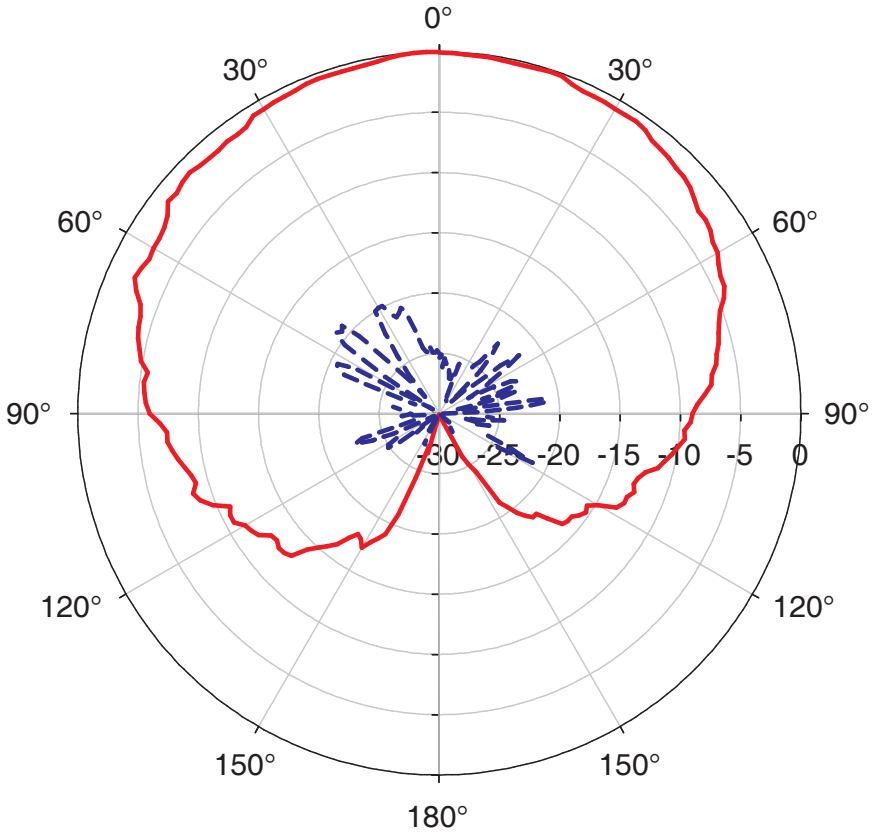

Figure 4-9: Measured E-Plane radiation pattern at 10.47 GHz

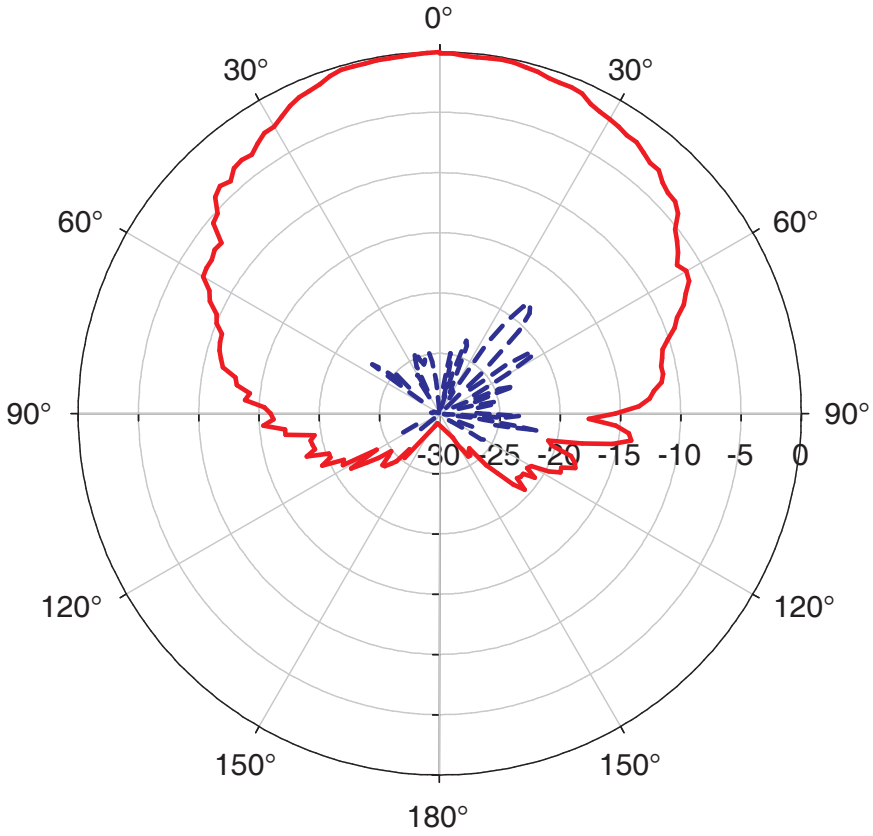

Figure 4-10: Measured H-plane radiation pattern at 10.47 GHz

Referring to Figure 4-7 - Figure 4-10, it can be seen that the SICBSA exhibits a very consistent hemispherical radiation pattern at the center frequency and at the second resonant frequency, confirming that polarization purity can be expected over the wide impedance bandwidth of the antenna.

To measure the gain of the SICBSA prototype, an X-band standard gain horn is used as the reference. An average measured gain of 5.3 dBi is exhibited near the first resonance of the antenna with a slight increase in gain observed as the frequency of operation is increased. The radiation efficiency of the antenna is calculated by comparing the measured gain and the modeled directivity. The measured and simulated gain, simulated directivity, and the calculated radiation efficiency are plotted in Figure 4-11. The radiation efficiency is approximated as the ratio of the measured gain to the simulated directivity.

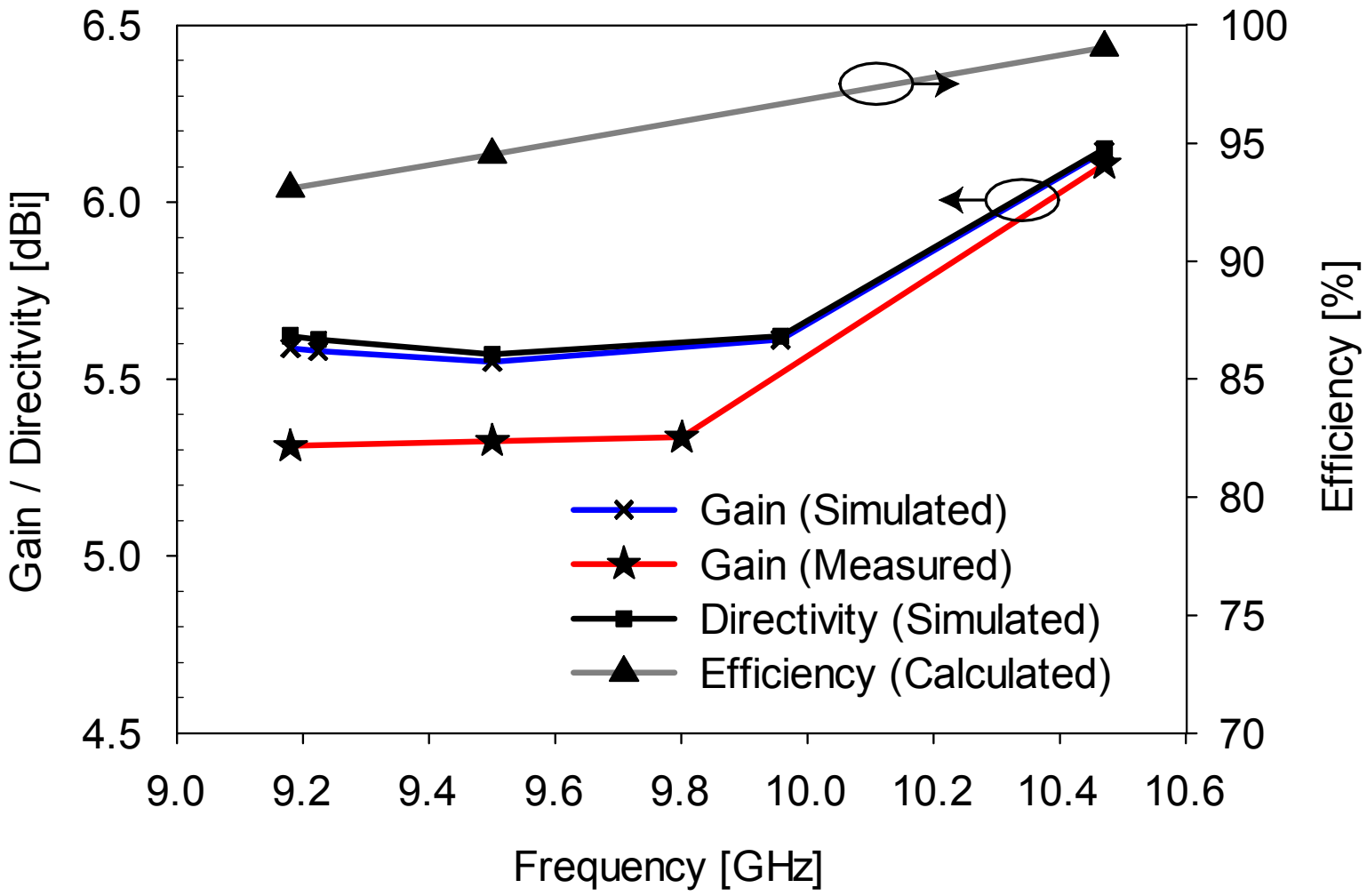

Figure 4-11: Measured and modeled gain, directivity, and calculated efficiency

0

CHAPTER 5: USE OF SICBSA AS AN ANTENNA ARRAY ELEMENT

5.1 SICBSA Array Overview

The proof-of-concept prototype demonstrates very good polarization purity, a hemispherical radiation pattern, and a uniform gain over a wide impedance bandwidth. Therefore, the next step is to investigate the SICBSA as the radiating element in an array configuration. It is well known that the spacing between array elements is a critical parameter in terms of array performance. When the spacing is very small, mutual coupling effects vastly alter the input impedance of the elements. This can be taken into account by redesigning the element to optimize the impedance including these effects. However, such an approach has obvious drawbacks including significantly more design effort (additional time and computational resources), and a possible reduction in the overall performance of the array. In order to avoid encountering these drawbacks, the element spacing can be increased in order to reduce or eliminate the effects of mutual coupling on input impedance. Again, one must be careful, as too large a spacing will result in the introduction of grating lobes [24]. These can occur in a phased array when the main beam is scanned off boresight if the spacing is between $0.5\lambda_0$- $1.0\lambda_0$. In addition, if the spacing is larger than $1.0\lambda_0$, grating lobes will occur even when the main beam is located at boresight (i.e. no phasing of input feeding signals). Grating lobes may be completely avoided if the size of an individual cell (element plus spacing) is less than or equal to $0.5\lambda_0$. However, keeping in mind that the element itself is approximately $0.5\lambda_0$, such a configuration is not practically possible. Therefore, an

optimal spacing must be determined for which mutual coupling effects are deemed negligible (namely that element redesign is not necessary to maintain performance).

5.2 Two Element Continuous Cavity DFCBSA Array

In order to determine the optimal spacing, a two element array is modeled in Ansoft HFSS. The study is carried out on the continuous cavity wall DFCBSA array shown in Figure 5-1 to reduce the required computational time. The determined value of spacing can then be applied to the SICBSA array show in Figure 5-2 for verification.

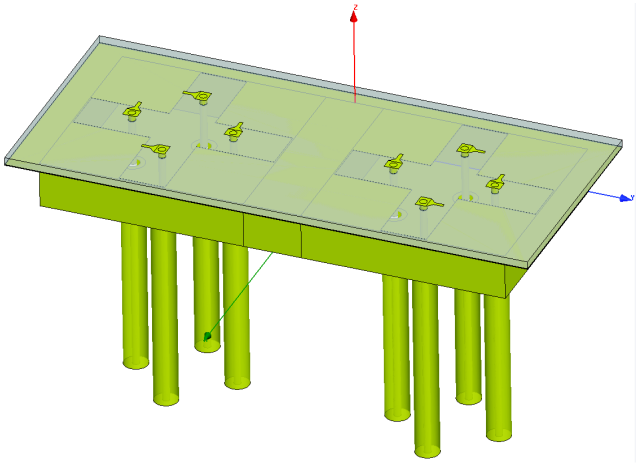

Figure 5-1: Two element continuous cavity DFBSA array

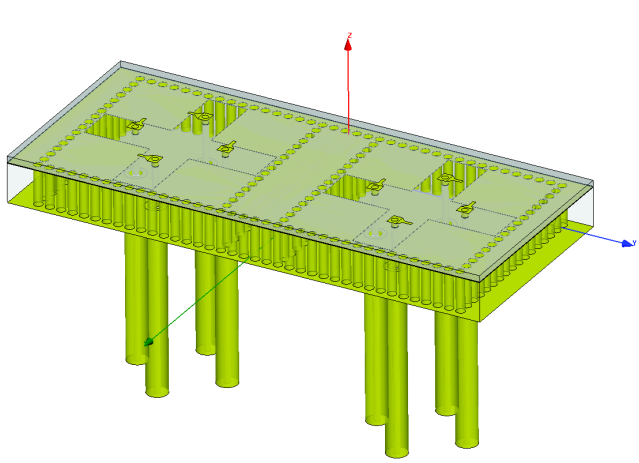

Figure 5-2: Two element differentially fed SICBSA array

The spacing between the elements, s_e , is initially minimized and subsequently increased gradually. For each value of element spacing, the S-parameters - which indicate matching (input impedance), individual element isolation (polarization), as well as inter-element isolation (coupling between elements) – and the radiation parameters are studied. The four-port S-parameters for one of the two elements (identical to those of

the second element) are shown in Figure 5-3 and Figure 5-4 for several different values of element spacing, s_e.

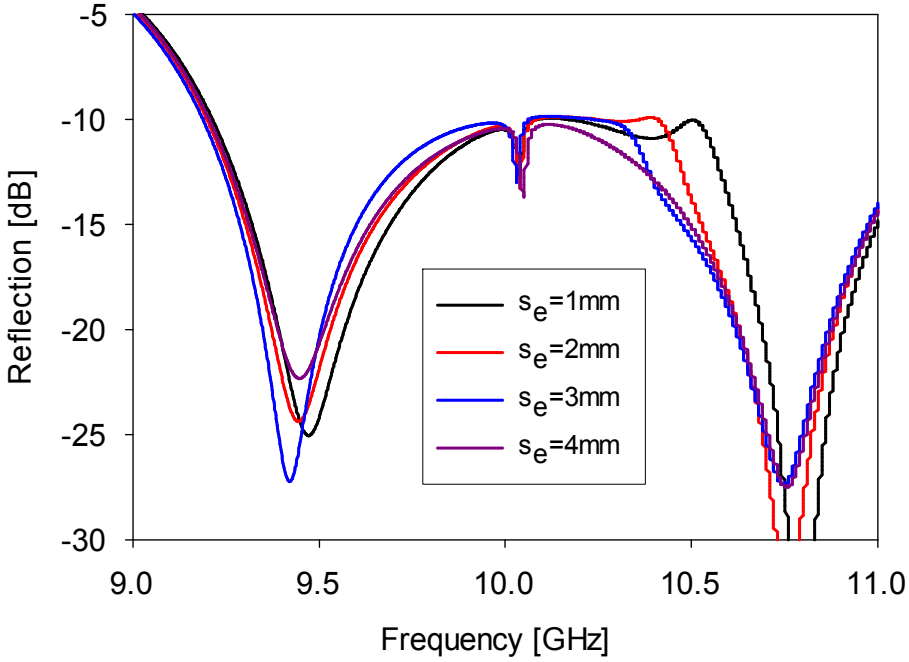

Figure 5-3: Reflection for two element continuous cavity DFCBSA array and different values of s_e

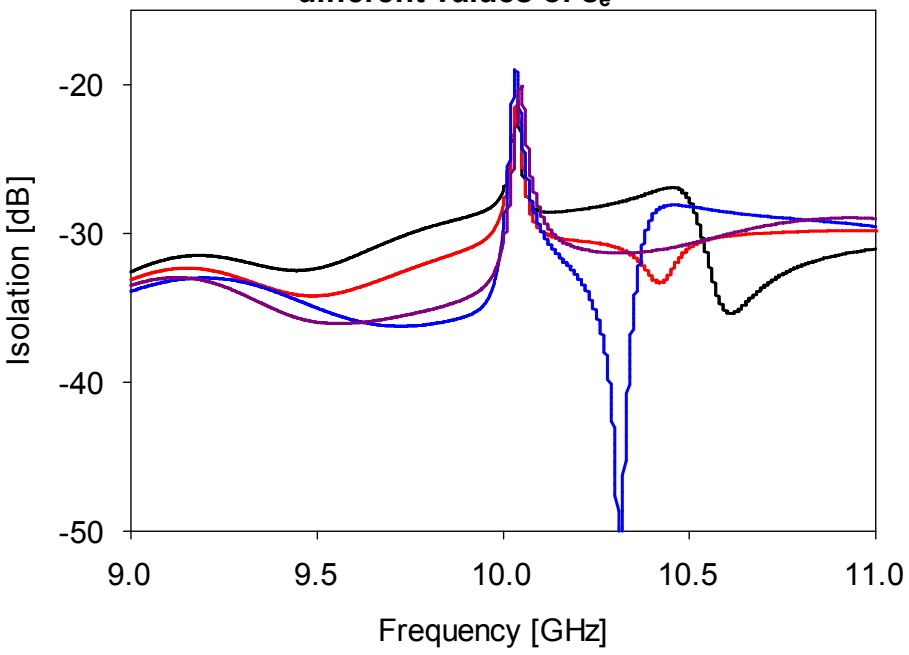

Figure 5-4: Isolation for two element continuous cavity DFCBSA and different values of s_e

It can be seen that a spacing of 4 mm (approximately $0.13\lambda_0$) results in a total unit cell size of $s_{cell} = L_c + s_e = 18\,mm,$ or $0.61\lambda_0$. In this configuration, there is almost no effect on the input reflection coefficients or isolation when compared with the single element case, as can be seen in Figure 5-5 where both sets of S-parameters are plotted together.

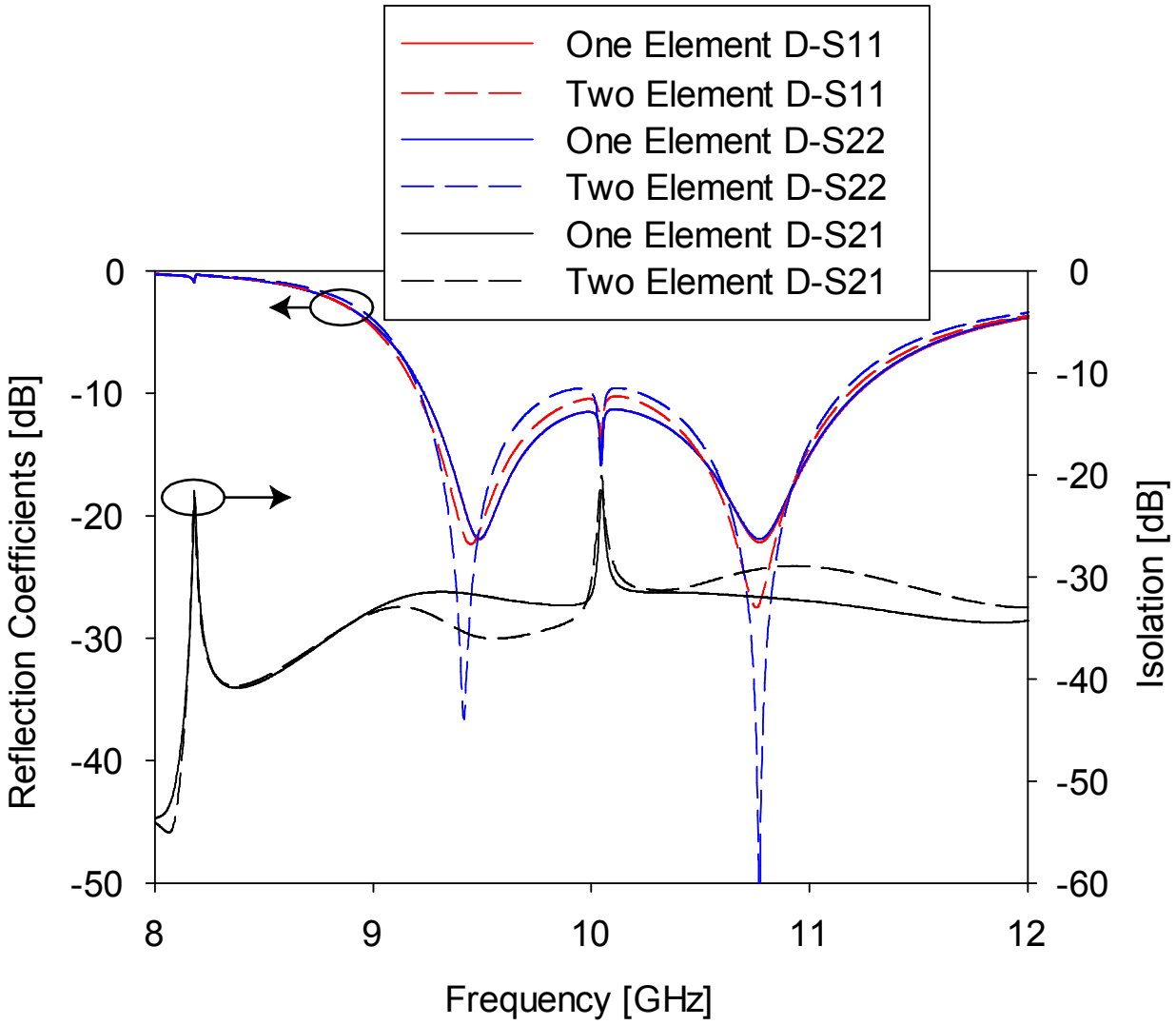

Figure 5-5: Reflection and isolation for one element and two element continuous cavity DFCBSA array

The radiation patterns are shown in Figure 5-6 - Figure 5-9. Referring to Figure 5-6 and Figure 5-7, where the array is aligned in the corresponding principle plane, the beam is seen to become narrower as expected [29]. When the cut is taken in the other principle plane (Figure 5-8 and Figure 5-9), the focusing effect of the array factor will not be observed. These radiation characteristics are discussed in more depth in the proceeding Section 5.3.

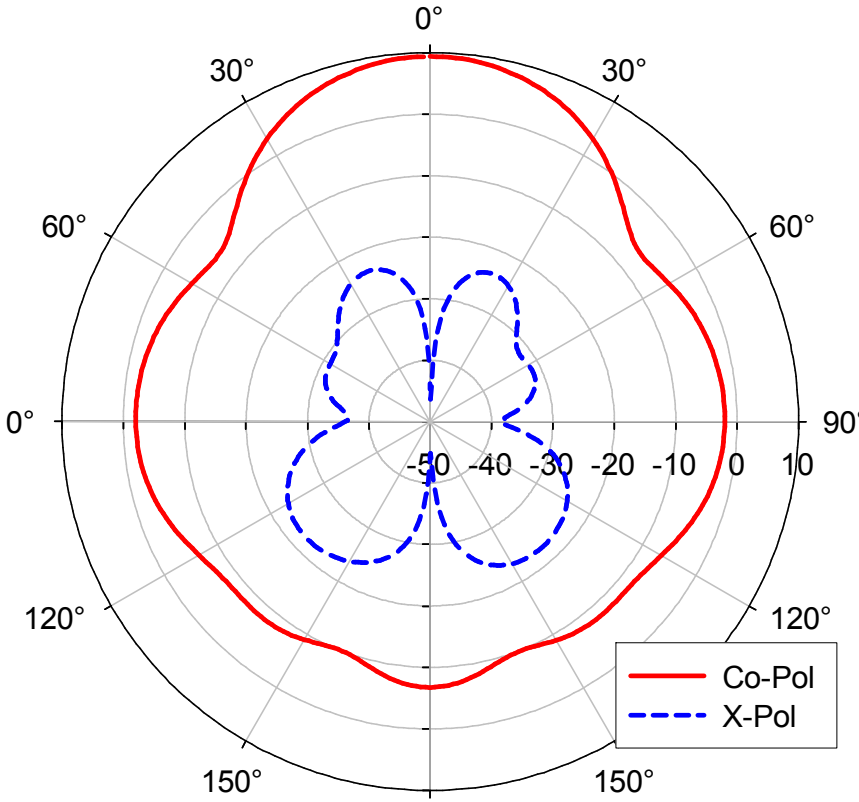

Figure 5-6: E-plane radiation pattern at 10 GHz (continuous cavity array aligned in E-plane)

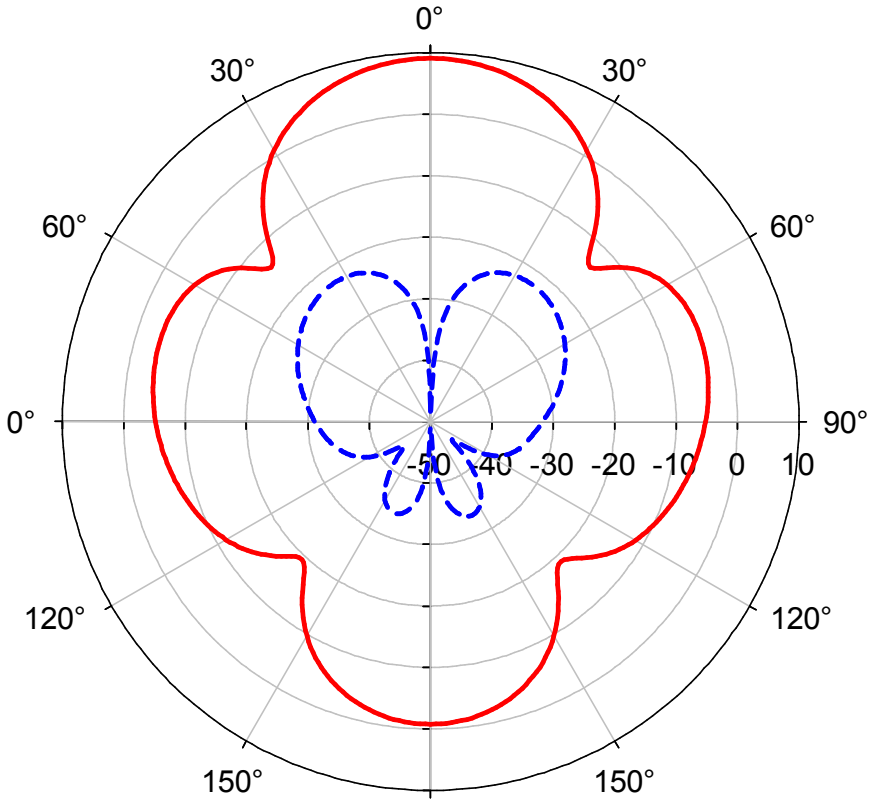

Figure 5-7: H-plane radiation pattern at 10 GHz (continuous cavity array aligned in H-plane)

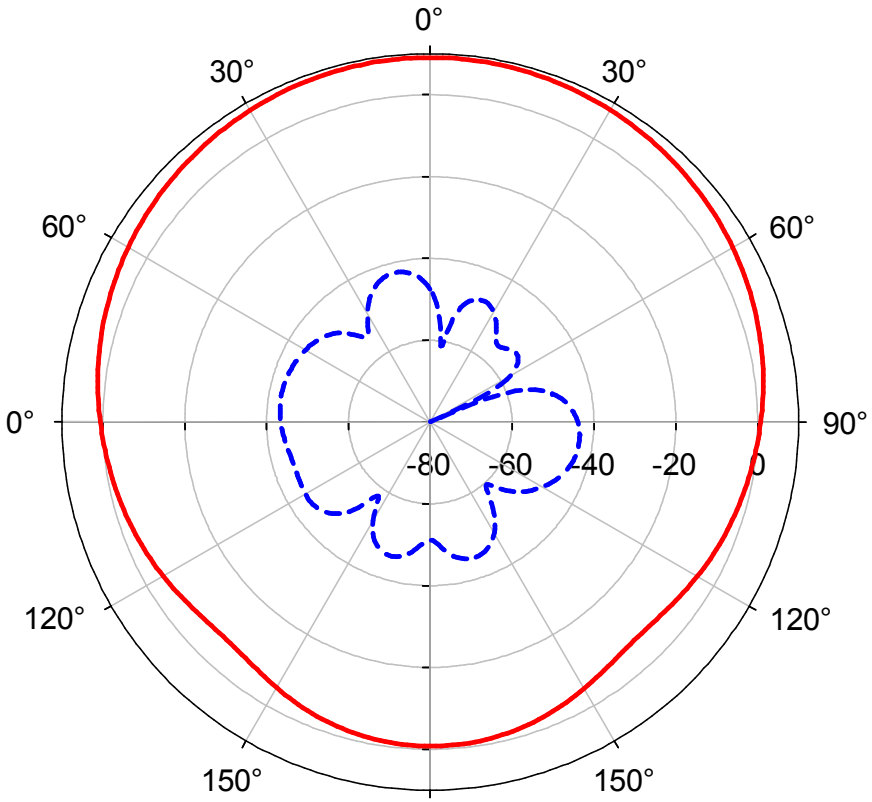

Figure 5-8: E-plane radiation pattern at 10 GHz (continuous cavity array aligned in H-plane)

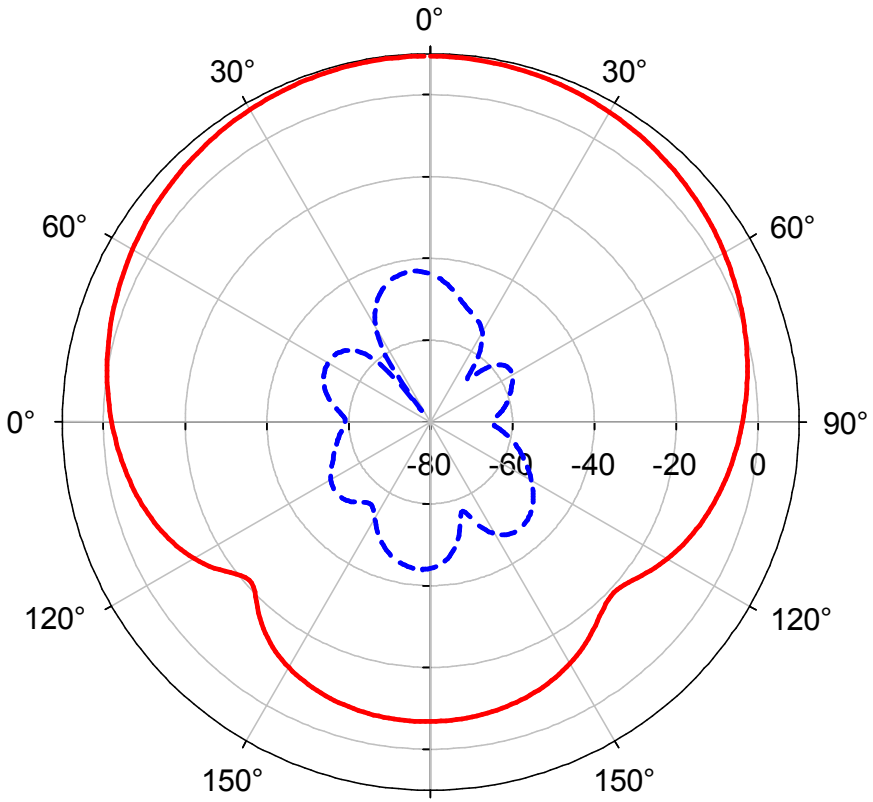

Figure 5-9: H-plane radiation pattern at 10 GHz (continuous cavity array aligned in E-plane)

5.3 Two Element SICBSA Array

The results of Section 5.2 verify the feasibility and demonstrate the performance of a continuous cavity DFCBSA linear array. However, it is observed that this topology is not practically achievable since it requires metal sheets to be located inside of the cavity substrate between adjacent elements. It is seen that when the continuous cavity wall is replaced with a SIW cavity, the attained differentially fed SICBSA array maintains similar performance. This topology (shown in Figure 5-2) is again simulated using Ansoft HFSS. The value of element spacing determined in Section 5.2 for the continuous cavity DFCBSA ($s_e = 4\,mm$) is expected to result in a similarly negligible level of mutual coupling if applied to the SICBSA array. However, the achievable element spacing for the SICBSA is limited to discrete values determined by the size and spacing of the vias used to form the cavity. A comparable element spacing value of $s_e = 5.3\,mm$ (yielding a unit cell size of $s_c = 0.65\lambda_0$) is used for the two element SICBSA array. This results in the input reflection and isolation displaying very little difference from the one element case, as shown in Figure 5-10. The two resonance and center frequencies are maintained, as is the bandwidth of 19%. A slight difference is observed in the degree to which matching is achieved, most notably at the center frequency, which has decreased from $D - S_{11} = -10\,dB$ to $-9.13\,dB$. However, this could be improved by a slight modification of the feed spacing if needed. The achieved input matching corresponds to a $VSWR \leq 2.074$ over the entire bandwidth, which is acceptable for many applications.

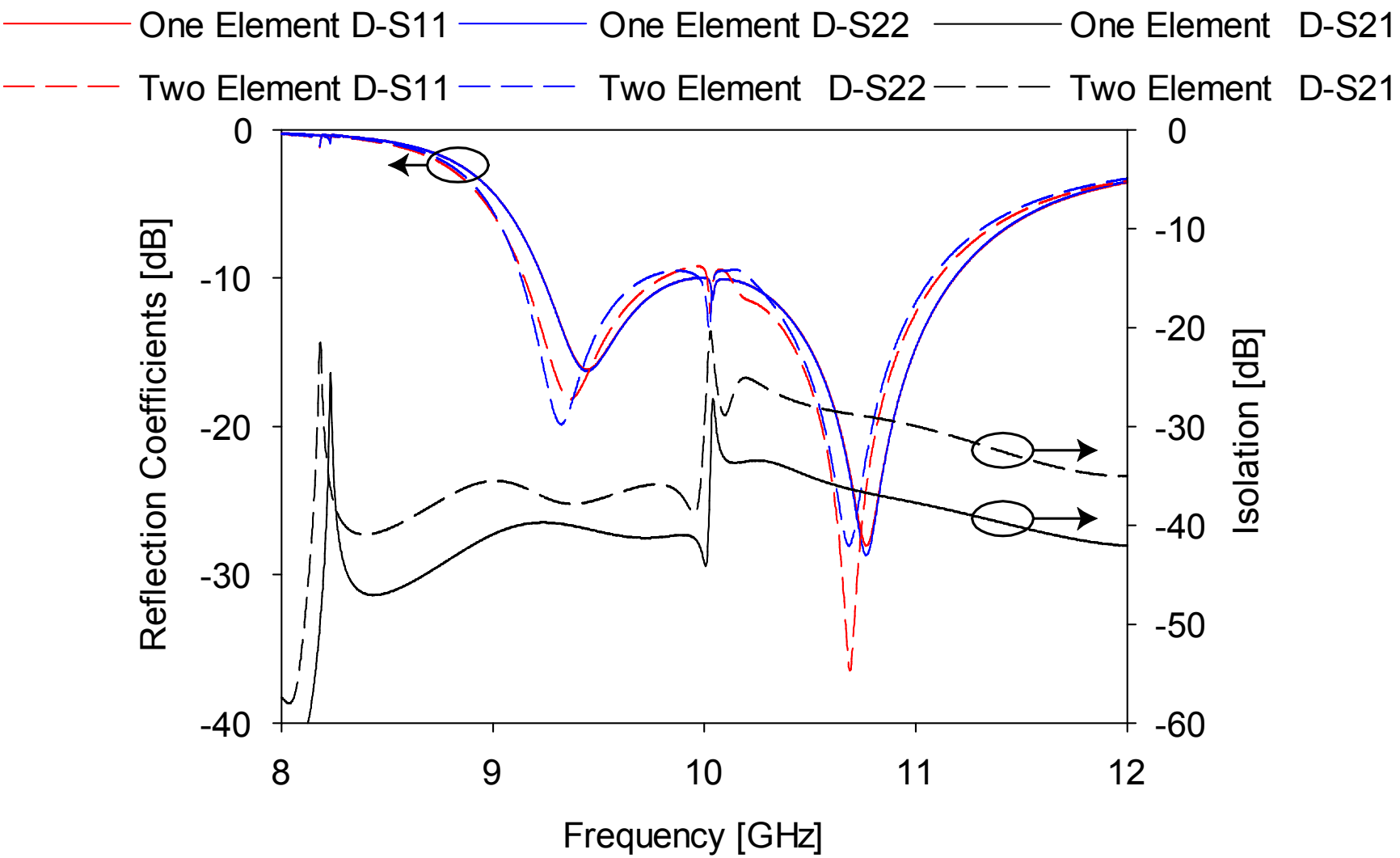

Figure 5-10: Reflection and isolation for one element and two element SICBSA array

The resulting radiation patterns are illustrated in Figure 5-11 - Figure 5-18. Once again, when the array is aligned in the corresponding principle plane, the beam becomes narrower. The increase in boresight gain can be compared with the expected theoretical gain increase by calculating the directivity of the array factor. An approximation for the directivity of an N-element broadside array is given by (5-1), where D_0 is the boresight directivity and d is the spacing between elements.

$$D_0 = 2N\left(\frac{d}{\lambda}\right) \tag{5-1}$$

For the two element SICBSA array, this yields:

$$D_0 = 2 * 2\left(\frac{0.65\lambda_0}{\lambda_0}\right) = 2.6 = 4.15\ dB \tag{5-2}$$

The expected gain for an N element array could be approximated by adding the calculated directivity of the array factor to the one element gain. The simulated one and two element SICBSA array gains are $G_{1-elem} = 5.7\ dBi$ and $G_{2-elem} = 9.4\ dBi$, yielding a difference of $3.7\ dB$. This compares reasonably well with the calculated value found in Equation (5-2). Further gain enhancement can be obtained by increasing the number of elements in the linear array. The expected gain for several different values of N are presented in Table 5-1, where calculations have been performed using the one element modeled gain and Equation (5-1).

Table 5-1: Predicted gain for N-element linear SICSA array

N	Gain [dBi]
1	5.7
2	9.57
3	11.33
4	12.58
5	13.55
10	16.56
20	19.57

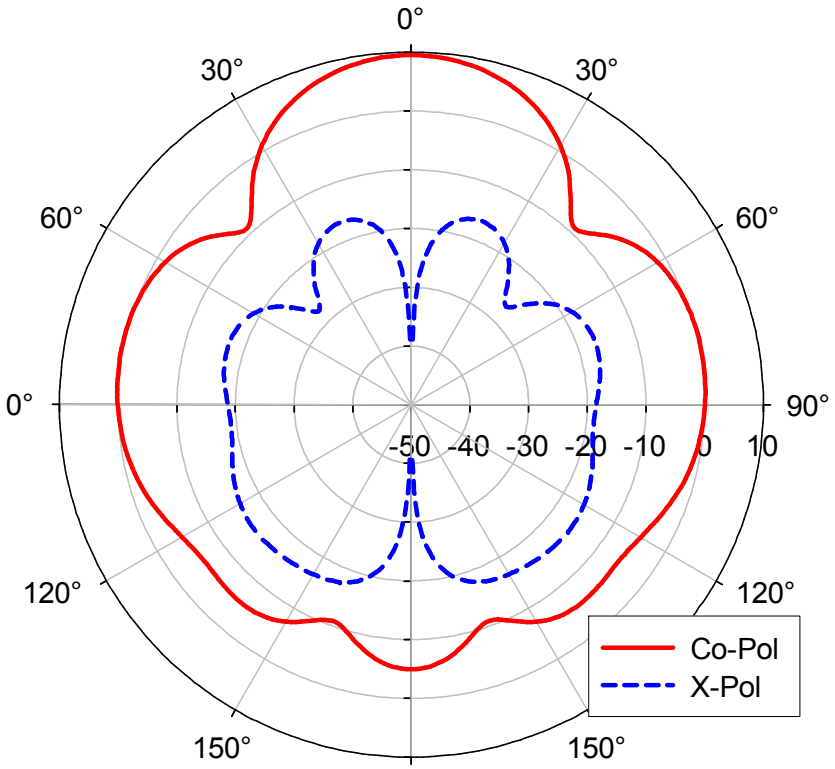

Figure 5-11: E-plane radiation pattern at 10 GHz (SICBSA array aligned in E-plane)

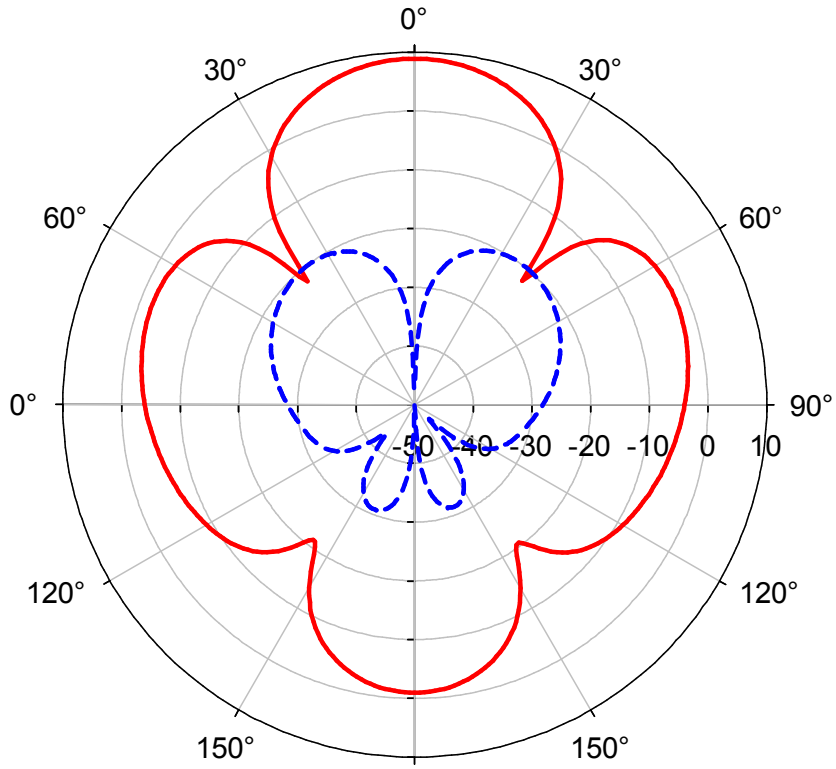

Figure 5-12: H-plane radiation pattern at 10 GHz (SICBSA array aligned in H-plane)

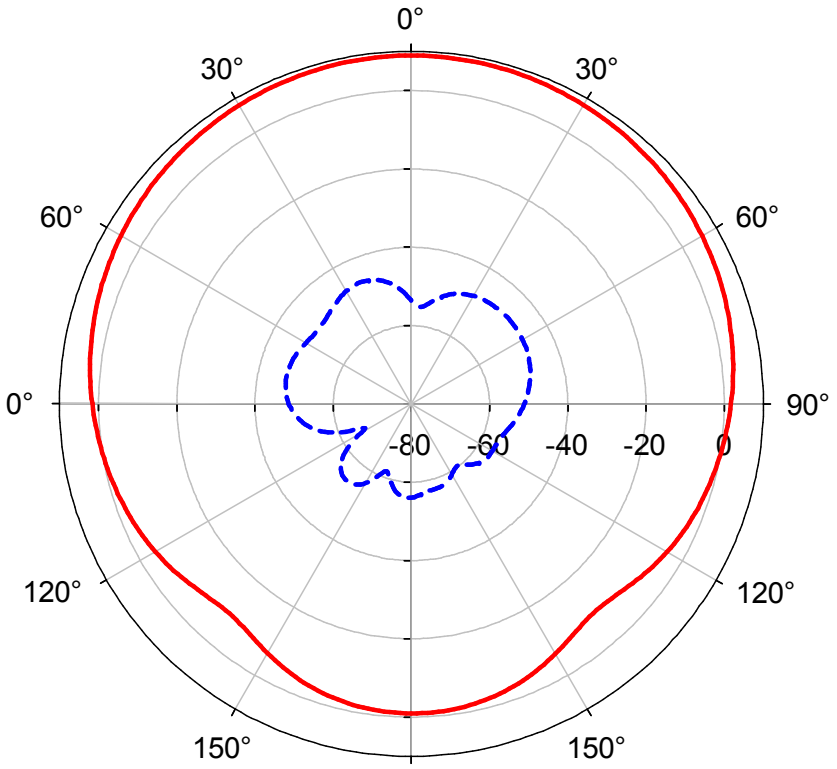

Figure 5-13: E-plane radiation pattern at 10 GHz (SICBSA array aligned in H-plane)

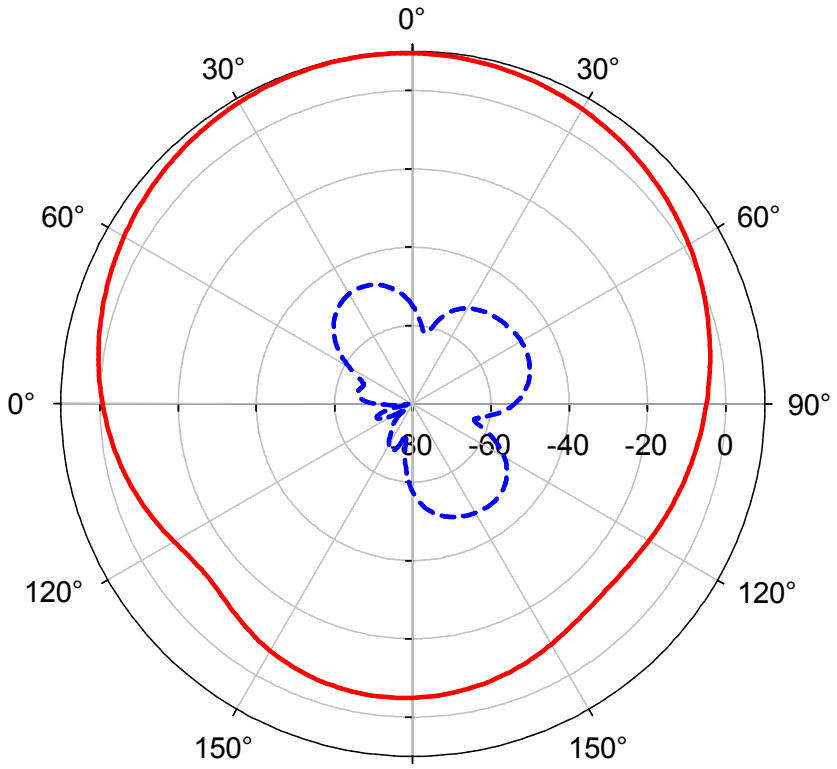

Figure 5-14: H-plane radiation pattern at 10 GHz (SICBSA array aligned in E-plane)

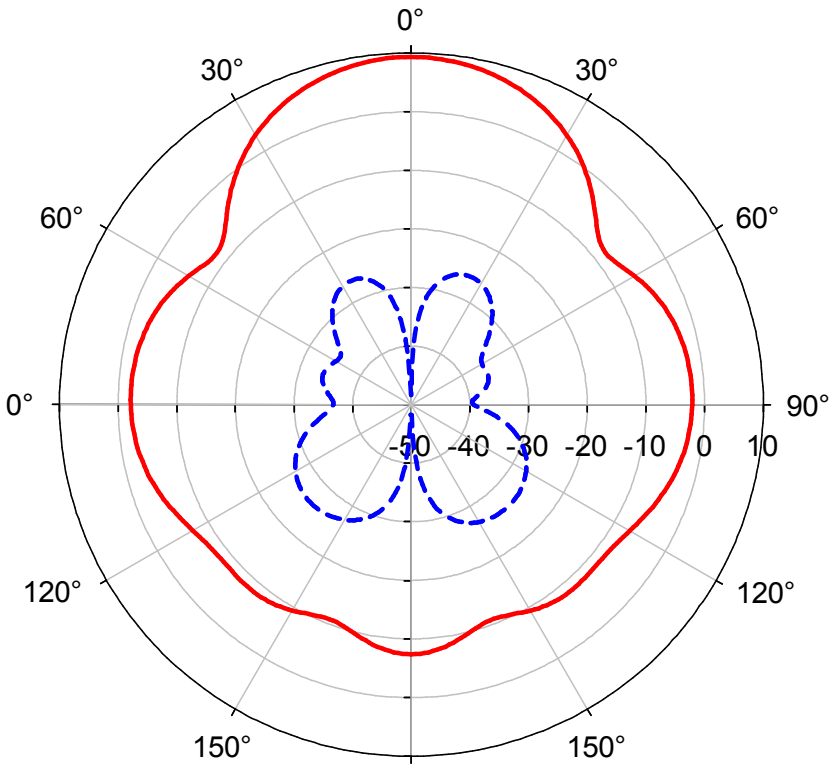

Figure 5-15: E-plane radiation pattern at 9.3 GHz (SICBSA array aligned in E-plane)

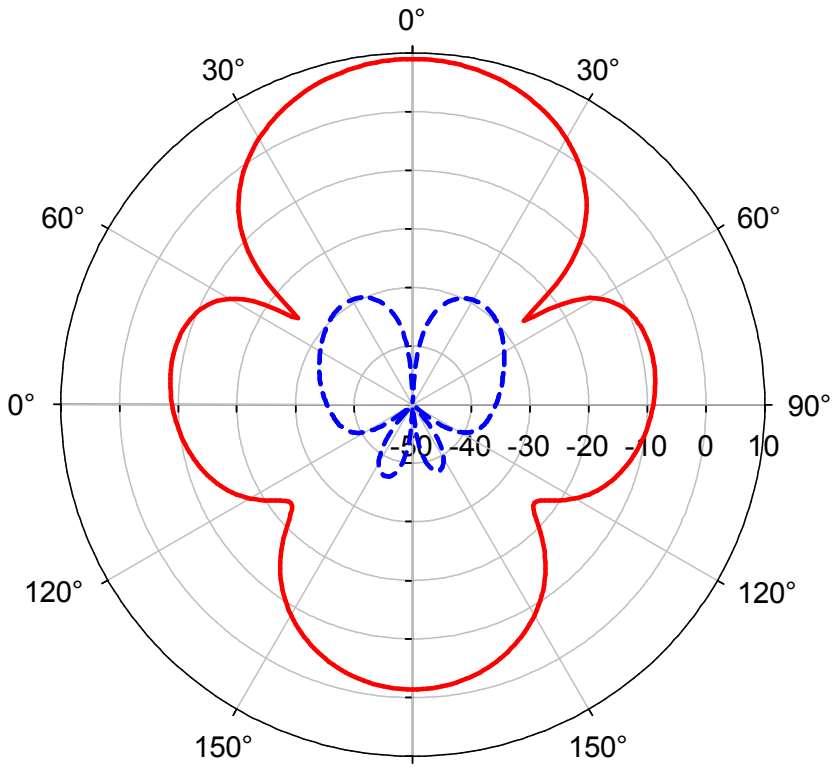

Figure 5-16: H-plane radiation pattern at 9.3 GHz (SICBSA array aligned in H-plane)

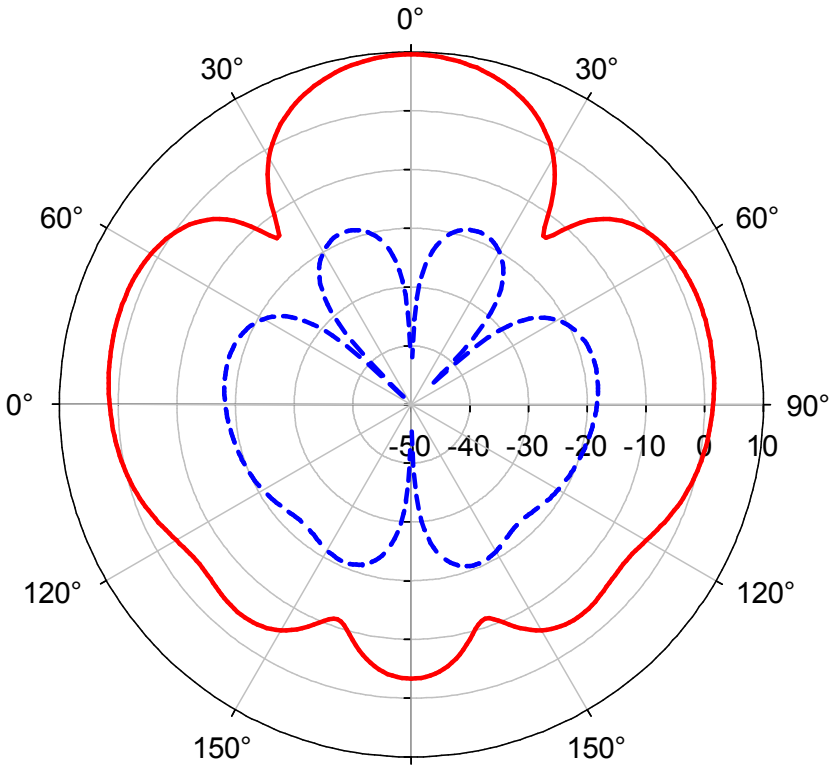

Figure 5-17: E-plane radiation pattern at 10.7 GHz (SICBSA array aligned in E-plane)

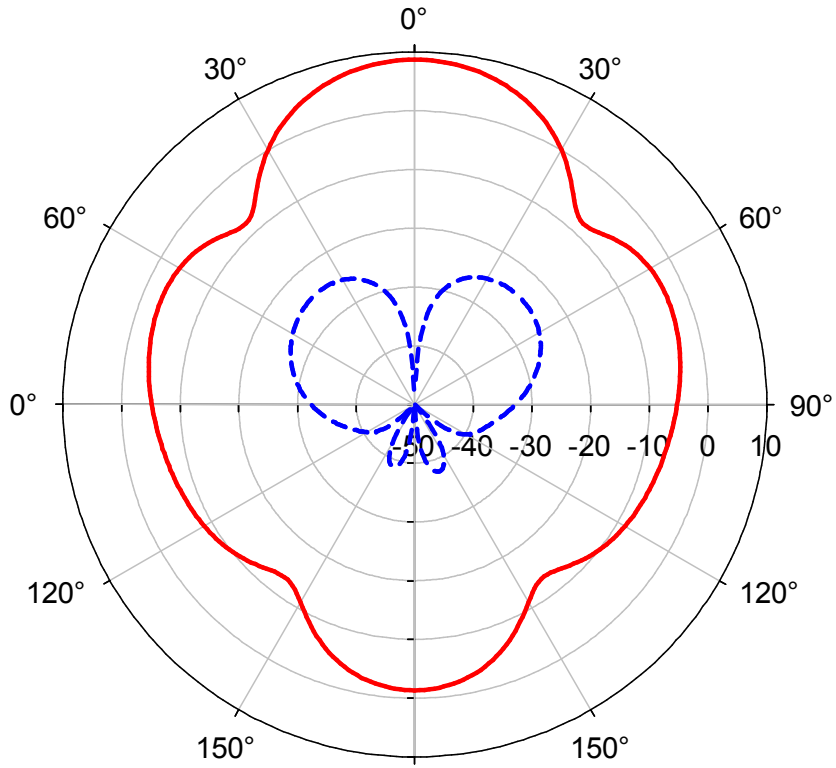

Figure 5-18: H-plane radiation pattern at 10.7 GHz (SICBSA array aligned in H-plane)

As shown in Figure 5-15 - Figure 5-18, the two element SICBSA array maintains its performance over the wide operational range. It is noted that at the second resonant frequency, 10.7 GHz, the E-plane pattern (Figure 5-17) becomes slightly more narrow than at the first resonant and center frequencies. In addition, the H-plane pattern (Figure 5-18) is slightly broader than at lower frequencies. While it is expected that the shaping of the array factor will vary with frequency, it is appropriate to verify that this particular trend is indeed expected. Hence a straightforward analysis of the array using its array factor is carried out. For a two element array of constant amplitude the array factor is given by Equation (5-3), where θ is the observation angle measured from the z-axis. The elements are assumed to be positioned along the z-axis, and fed with a phase separation β, which is zero for the present case since the elements are fed in phase.

$$AF = 2\cos\left[\frac{1}{2}(kd\cos\theta + \beta)\right] \tag{5-3}$$

The array factor formulation does not take into account the effects of mutual coupling between the antenna elements, so it will not predict the exact response of the array. However, for a unit cell size of at least 0.5λ, the calculated array factor should provide a reasonable approximation to the total array pattern. Therefore, the simulated electric field patterns for the single element SICBSA at the center frequency as well as at the first and second resonant frequencies are exported from HFSS. The array factor is calculated at each frequency based on the spacing between unit cells. The calculated and simulated total electric field intensity (linear magnitude) patterns at each frequency

are given in Figure 5-19 – Figure 5-24. It can be seen that the calculated array patterns are in very good agreement with the simulated patterns. The discrepancies primarily occur at the side and back lobes, where it is expected that the effects of mutual coupling between antennas will be the most prominent. The observed variations can be understood as very small when the scaling of the linear intensity is considered. The predicted E-plane and H-plane total electric field patterns shown in Figure 5-23 and Figure 5-24 are closely matched to their corresponding simulations. This indicates that the observed far field patterns in Figure 5-17 and Figure 5-18 are correct, and not the result of unexpected behavior. The differentially fed SICBSA is next demonstrated in a uniform two element phased array in the proceeding Section 5.4.

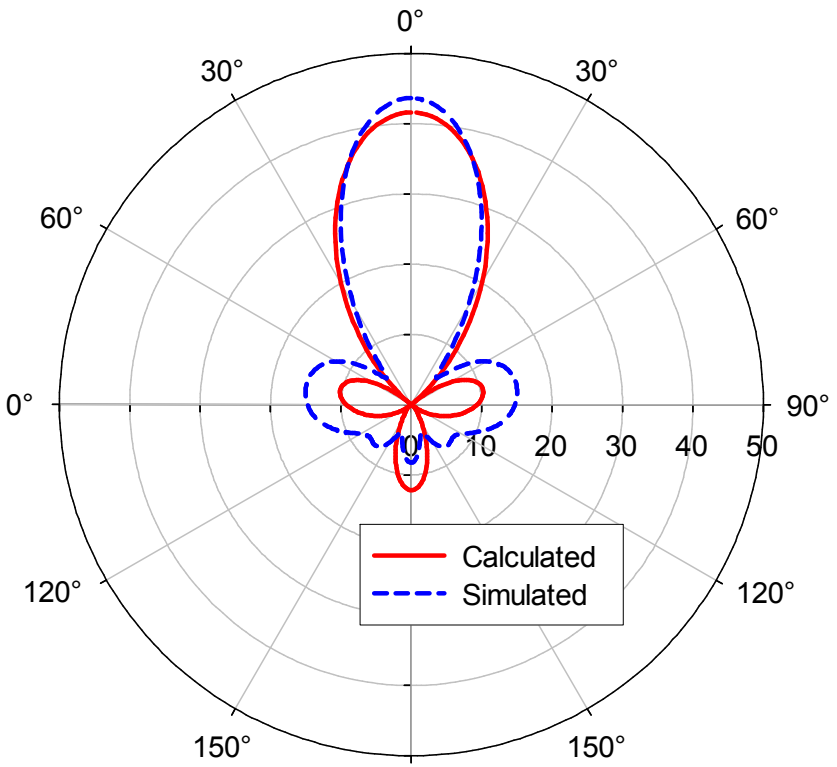

Figure 5-19: Total electric field intensity in the E-plane at 10 GHz (SICBSA array aligned in E-plane)

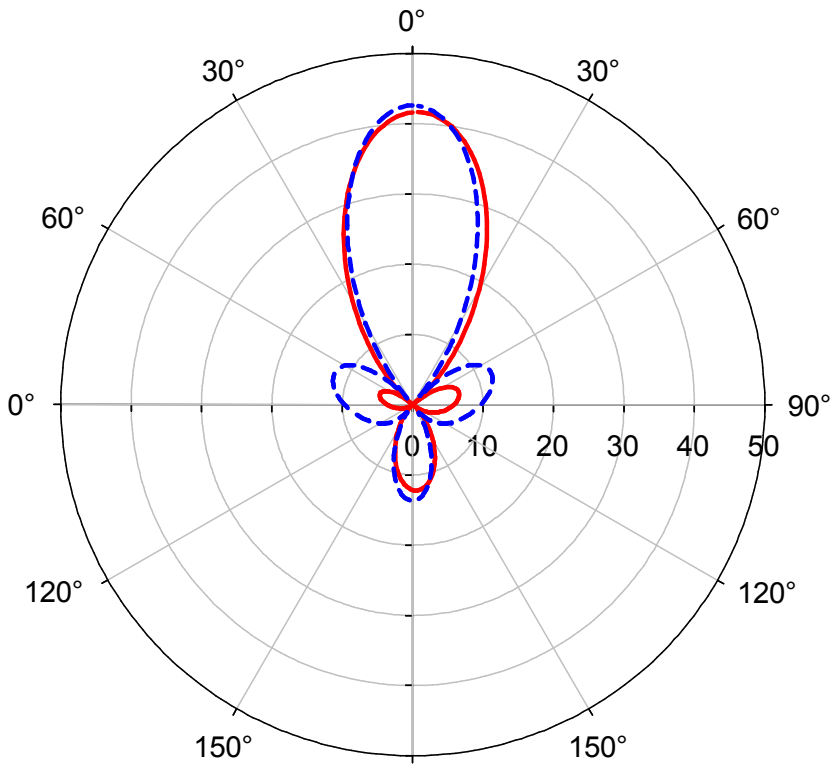

Figure 5-20: Total electric field intensity in the H-plane at 10 GHz (SICBSA array aligned in H-plane)

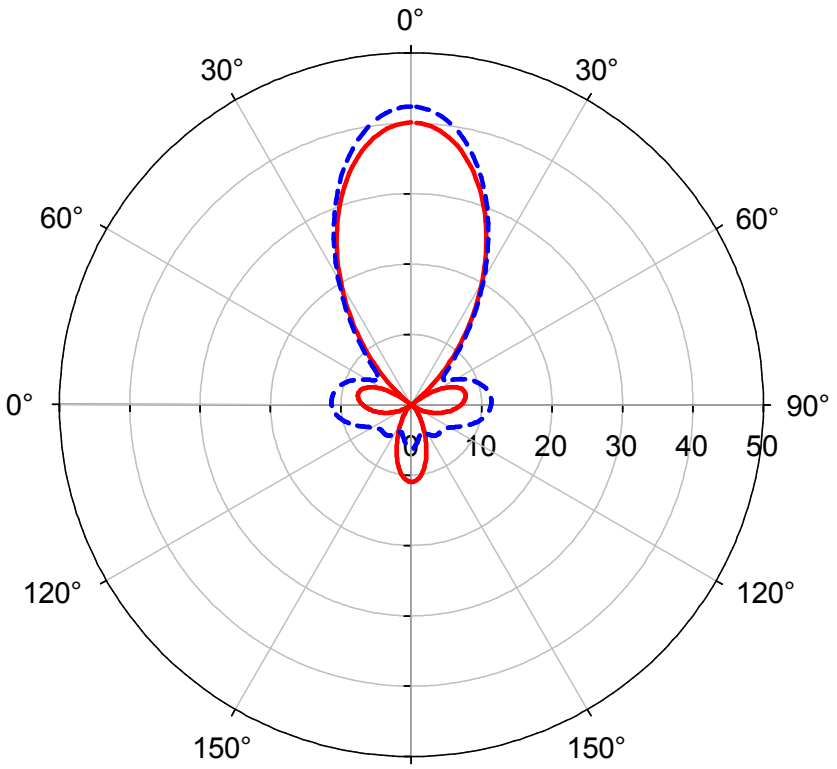

Figure 5-21: Total electric field intensity in the E-plane at 9.3 GHz (SICBSA array aligned in E-plane)

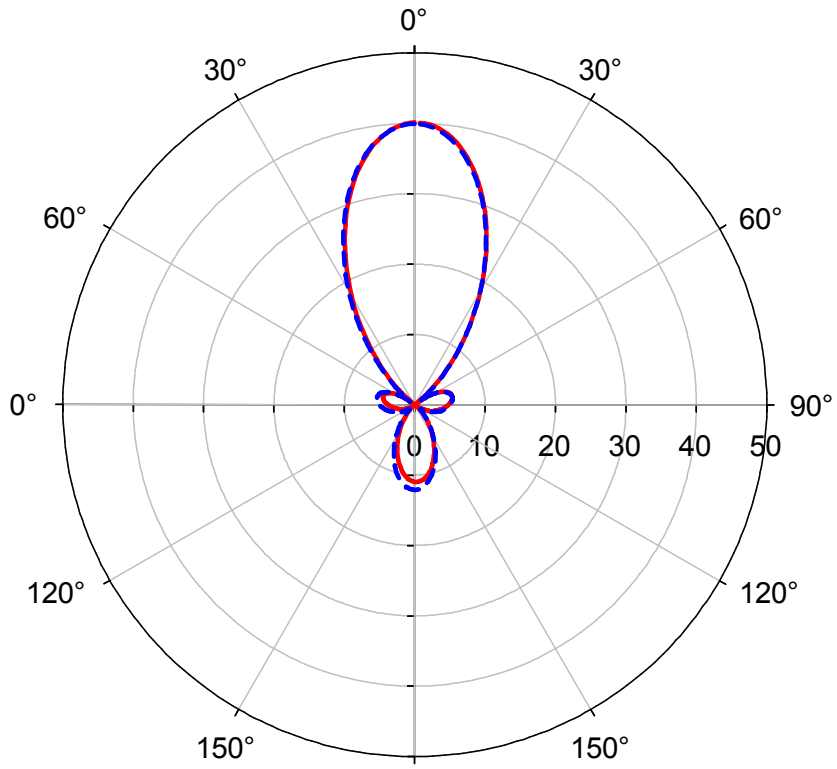

Figure 5-22: Total electric field Intensity in the H-plane at 9.3 GHz (SICBSA array aligned in H-plane)

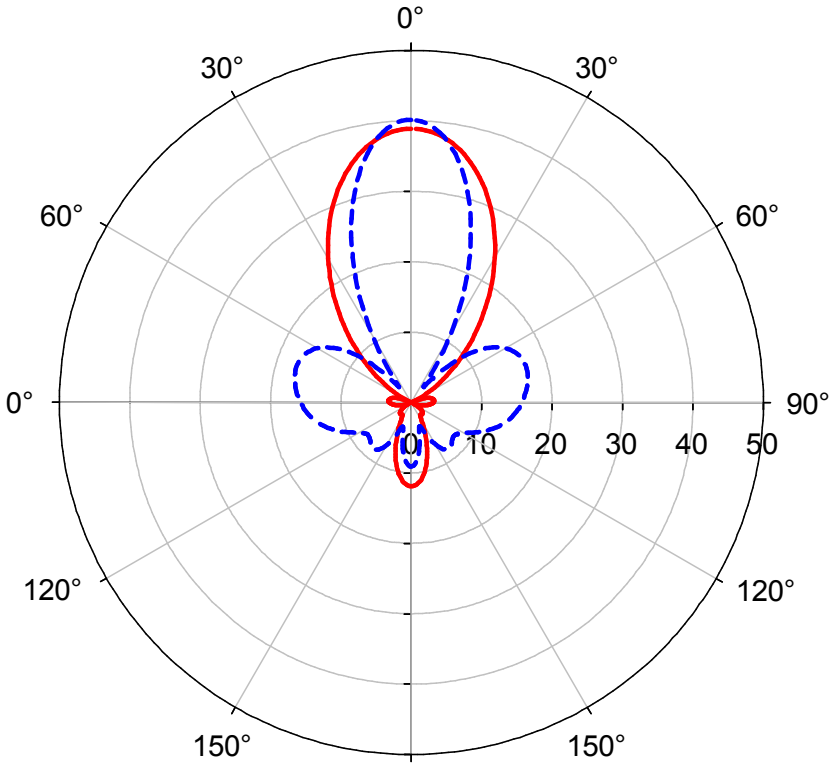

Figure 5-23: Total electric field intensity in the E-plane at 10.7 GHz (SICBSA array aligned in E-plane)

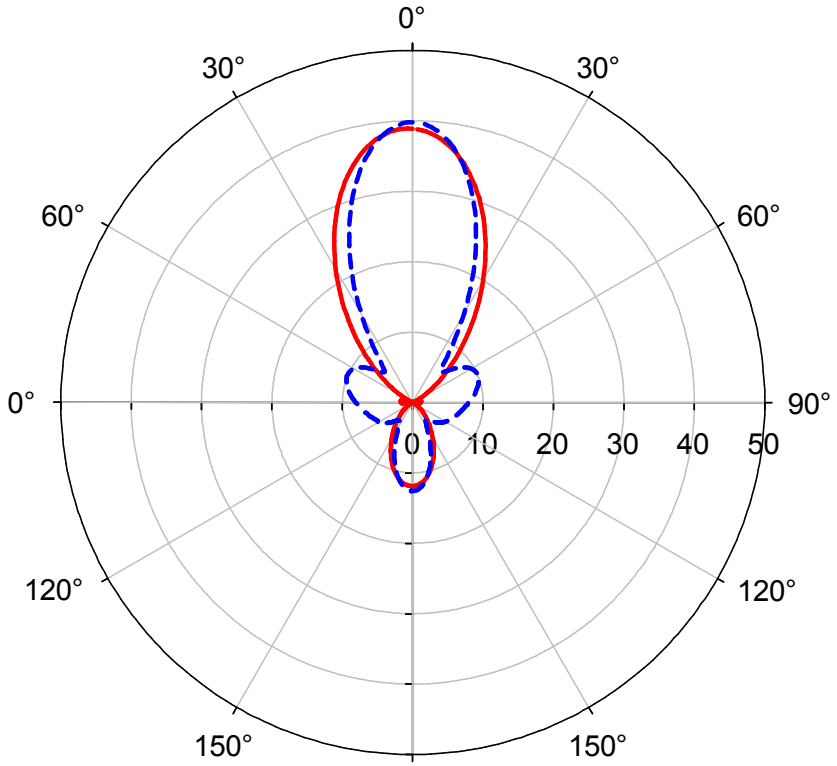

Figure 5-24: Total electric field intensity in the H-plane at 10.7 GHz (SICBSA array aligned in H-plane)

5.4 Uniform Two Element SICBSA Phased Array

The linear array results presented in Section 5.3 indicate that the SICBSA should be suitable for common antenna array applications including use in a phased array. The feasibility may be tested by extending the differentially fed SICBSA results to investigate the effects of feeding on the direction of radiation. It is well known that a linear array of elements can be used for beam scanning when a simple phasing of the input signals is applied. The direction of the array factor main beam , θ_0, is related to the applied phase difference , β, by the following relationship.

$$\psi = kd\cos\theta + \beta|_{\theta=\theta_0} = kd\cos\theta_0 + \beta \Rightarrow \beta = -kd\cos\theta \qquad (5\text{-}4)$$

Figure 5-25, illustrates the main beam of the antenna is relocated from its previous boresight location to an angle of $\theta_0 = 5°$. In this case the applied phase separation was $\beta = 35°$. In Figure 5-26, a phase separation $\beta = 143°$ in the E-Plane and $\beta = 160°$ in the H-Plane is applied, in order to locate the main beams in each principle plane at $\theta_0 = 30°$.

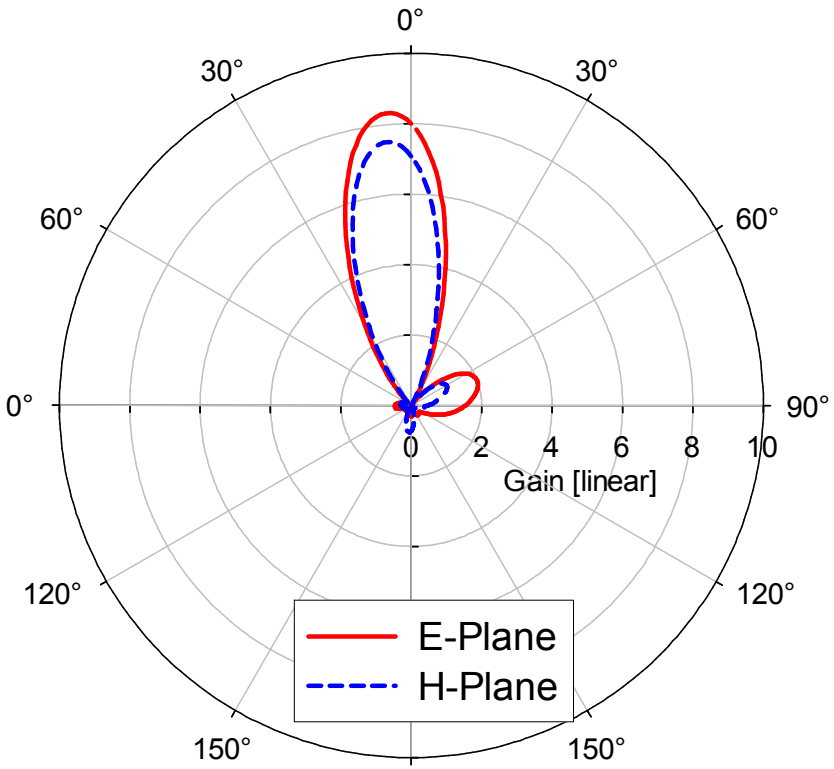

Figure 5-25: SICBSA phased array radiation pattern at 10 GHz, beam at 5˚

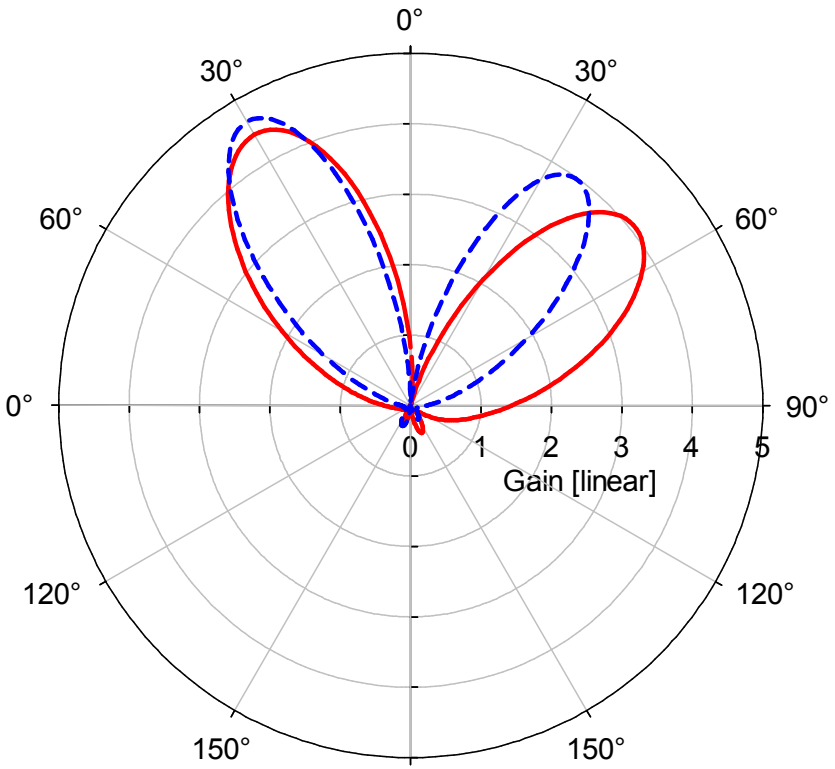

Figure 5-26: SICBSA phased array radiation pattern at 10 GHz, beam at 30˚

It can be seen, that as the beam is located further from boresight, the side lobe level increases. The level of the side lobe in a linear array may be controlled by using a non-uniform amplitude distribution, as discussed in [24] and other literature.

The differentially fed SICBSA array appears to be a feasible phased array element. As such, it may be suitable for a multitude of electronically steerable array (ESA) applications including various types of radar systems, direction of arrival (DOA) estimation systems, and communications systems. Implementing the SICBSA in such configurations will require control over the feeding of the antenna elements. For example, the 180° phase shifts required for differential feeding, may be accompanied by 90° phase shifters if circular polarization is desired, as well as additional phase shifters to accommodate element phasing for a desired beam pattern. For a large number of elements, this may lead to a complex feeding network which is beyond the scope of this dissertation. However, it is worth discussing potential implementation of the required feeding networks as a demonstration of the DFCBSA array topology's potential usefulness in these types of configurations. Such a discussion is presented in the next section.

5.5 Feed Network & Phase Shifters

As discussed in Section 2.2, the dual polarized differentially fed SICBSA antenna requires four feeds. To accommodate the dual differential feeding scheme (illustrated in Figure 3-4), the ideal feed will integrate a wideband differential feeding network which can be utilized for each polarization feed of the antenna. In addition, when used as an array element there will be associated feed circuitry required for power splitting, and if

used in a phased array, additional phase shifters will be required between elements. Traditionally, such feeding networks are heavy, expensive, require a large area, and are difficult to design. In addition, the overall matching of the system will be impacted by how well the feed network and antenna are matched to the input source.

The design and implementation of such a feed network is beyond the scope of this dissertation. As a basic consideration, though, the following comments address the practical issues concerning the possible solutions to developing a feed network of this type. There are several types of current implementations to wideband differential power splitting. Typically active devices are employed to achieve very wideband performance. However, it is noted that several novel and light-weight types of components have been reported in recent years that could be used to design and build such phase shifters. These include ferroelectric tunable devices such as Barium Strontium Titanate (BST) thin film phase shifters, which have been demonstrated in various configurations. These types of phase shifters have several advantages over current ferrite, MMIC, or MEMS phase shifters. This includes quick switching speeds (ferrite phase shifters slowly respond to their control circuits) which would be particularly useful in fast scanning applications including tracking array antennas. MEMS and MMIC phase shifters do not suffer from slow switching, but have limited power handling capabilities which are overcome by ferroelectrics. In addition, ferroelectric phase shifters will have a reduced loss (compared with MEMS devices, which have higher losses in the microwave region). Ferroelectric based phase shifters have their own shortcomings including high tuning voltages, and high conductor loss due to the high dielectric constant of the

material. With recent advancements in the processing of these materials, these issues seem likely to be reduced or resolved.

Another recent class of phase shifters which may be used to construct wideband differential power splitters are made from so called composite right/left-handed (CRLH) metamaterials. These topologies can provide a specified wideband phase shift in a very small area using simple printed circuit technology such as microstrip lines. A variety of different variations been reported in the literature.

Finally, and perhaps most simply, a variety of transmission line transition type differential power splitters have been reported in recent years. These topologies work by providing a transition from an initial topology which is simple to excite (such as a microstrip line) to another, inherently differential, type of transmission line such as a coplanar waveguide (CPW) or coplanar strips (CPS). These topologies might be the best type to integrate with SICBSA, due to the possibility of directly integrating the planar feeding circuit with the antenna stackup. For example, the four feeding via contact points beneath the cavity could be connected to planar printed circuit transmission lines which are a part of the wideband differential feeding circuit. In this case, the antenna could retain its current low profile, and very little would be added to the cost and weight of the total system. In addition, since printed circuits would be used tuning might be accomplished in the same manner as demonstrated in this dissertation.

CHAPTER 6: CONCLUSIONS

The focus of this dissertation was to develop and demonstrate a dual-polarized antenna with a wide impedance bandwidth, wideband polarization purity, compact size, and a simple design procedure. A cavity backed crossed slot was chosen to obtain a wideband response, high radiation efficiency, hemispherical radiation patterns, and to reduce the propagation of surface waves. In order to maintain good isolation between the orthogonal radiators, a dual differential feeding structure was developed. The probe fed microstrip line feeds allow the antenna designer to take advantage of a tunable dual resonance to obtain a wideband impedance match of approximately 20% and obtain a wideband isolation of 30 dB. The antenna displays wideband polarization purity, exhibiting very consistent radiation patterns, relatively consistent gain, and a very high radiation efficiency of above 95% over its operating range. The antenna can operate in either vertical polarized, horizontal polarized, dual linear polarized or circular-polarized modes.

In order to facilitate standard fabrication techniques and allow the antenna to be used in arrays, the antenna is demonstrated using a substrate integrated waveguide cavity. The effects of mutual coupling have been studied in order to determine a practical value for element spacing in an array. The performance of a two element uniform linear array has been demonstrated in simulations, where a 20% bandwidth is maintained while achieving an increased gain and focused array patterns. A simple phased array is simulated to demonstrate scanning of the main beam of the array from boresight to thirty degrees. Potential candidates for an integrated wideband differential

feed network and phase shifters for use in an array have been proposed as future work. In such a configuration, the removal of the coaxial cables will lead to a much lower profile and increase the practicality of using the antenna in very compact planar applications.

The developed wideband dual-polarized SICBSA is widely suitable for a multitude of applications such as mobile telephony, broadband MIMO communications systems, wireless local area network (WLAN) communications, polarization diversity systems, and for use as an array element. In an array configuration, the dual-polarized nature lends to a number of significant applications including spacecraft and aircraft tracking, direction-of-arrival estimation, adaptive beamforming, and numerous radar configurations.

LIST OF REFERENCES

[1] G. H. Knittel, A. Hessel, and A. A. Oliner, “Element Pattern Nulls in Phased Arrays and Their Relation to Guided Waves,” Proc. IEEE, vol. 56, pp. 1822–1836, Nov. 1968.

[2] D. M. Pozar and D. H. Schaubert, “Scan Blindness in Infinite Phased Arrays of Printed Dipoles,” IEEE Trans. Antennas Propag., vol. 32, pp. 602–610, Jun. 1984.

[3] D. M. Pozar, “Scanning Characteristics of Infinite Arrays of Printed Antenna Subarrays,” IEEE Trans. Antennas Propag., vol. 40, pp. 666–674, Jun. 1992.

[4] Y. Fu and N. Yuan, “Elimination of Scan Blindness in Phased Array of Microstrip Patches Using Electromagnetic Bandgap Materials,” IEEE Antennas Wireless Propag. Lett., vol. 3, pp. 63–65, 2004.

[5] A. Adrian and D. H. Schaubert, “Dual aperture-coupled microstrip antenna for dual or circular polarization,” Electron. Lett., vol. 23, pp. 1226–1228, Nov. 1987.

[6] S. D. Targonski and D. M. Pozar, “Design of wideband circularly polarized aperture-coupled microstrip antennas,” IEEE Trans. Antennas Propag., vol. 41, pp. 214–220, Feb. 1993.

[7] K. L. Lau and K. M. Luk, “A novel wide-band circularly polarized patch antenna based on l-probe and aperture-coupling techniques,” IEEE Trans. Antennas Propag., vol. 53, pp. 898–900, Jan. 2005.

[8] K. L. Wong and T. W. Chiou, “Broad-band single-patch circularly polarized microstrip antenna with dual capacitively coupled feeds,” IEEE Trans. Antennas Propag., vol. 49, pp. 898–900, Jan. 2001.

[9] S. Gao, L. W. Li, M. S. Leong, and T. S. Yeo, “A broad-band dual-polarized microstrip patch antenna with aperture coupling,” IEEE Trans.
Antennas Propag., vol. 51, pp. 898–900, Apr. 2003.

[10] C. H. Tsao, Y. M. Hwang, F. Killburg, and F. Dietrich, “Aperture-coupled patch antennas with wide-bandwidth and dual-polarization capabilities,” in IEEE Antennas and Propagation Symp. Dig., Syracuse, NY, USA, Jun. 1988, pp. 936–939.

[11] D. M. Pozar and S. M. Duffy, “A dual-band circularly polarized aperture-coupled stacked microstrip antenna for global positioning satellite,” IEEE Trans. Antennas Propag., vol. 45, pp. 1618–1625, Nov. 1997.

[12] N. Behdad and K. Sarabandi, “Wideband double-element ring slot antenna,” Electronics Letters, vol. 40, pp. 408–409, 2004.

[13] R. J. Mailloux, “On the use of metallized *[sic]* cavities in printed slot arrays with dielectric substrates,” IEEE Trans. Antennas Propag., vol. 35, pp. 477–487, May 1987.

[14] C. A. Lindberg, “A shallow-cavity uhf crossed-slot antenna,” IEEE Trans. Antennas Propag., vol. 17, pp. 558–563, Sep. 1969.

[15] H. E. King and J. L. Wong, “A shallow ridged-cavity crossed-slot antenna for the 240- to 400-mhz frequency range,” IEEE Trans. Antennas Propag., vol. 23, pp. 687–689, Sep. 1975.

[16] H. H. Chung, W. Foy, and S. Y. Peng, “Msat-x phased array crossed-slot element design,” in IEEE Antennas and Propagation Symp. Dig., Jun. 1987, pp. 356–359.

[17] N. T. Kazaross, H. H. Chung, and S. Y. Peng, “Improvement of crossed-slot element design for msat-x applications,” in IEEE Antennas and Propagation Symp. Dig., San Jose, CA, USA, Jun. 1989, pp. 1336–1339.

[18] F. Manshadi, “End-loaded crossed-slot radiating elements,” IEEE Trans. Antennas Propag., vol. 39, pp. 1237–1240, Aug. 1991.

[19] D. Sievenpiper, H. P. Hsu, and R. M. Riley, “Low-profile cavity-backed crossed-slot antenna with a single-probe feed designed for 2.34-ghz satellite radio applications,” IEEE Trans. Antennas Propag., vol. 52, pp. 873–879, Mar. 2004.

[20] Z. Shen, C. T. Sze, and C. L. Law, “A circularly polarized microstrip-fed t-slot antenna,” in IEEE Antennas and Propagation Symp. Dig., Salt Lake City, UT, USA, Jul. 2000, pp. 1008–1010.

[21] K. F. Tong and T. P. Wong, “Circularly polarized u-slot antenna,” IEEE Trans. Antennas Propag., vol. 55, pp. 2382–2385, Aug. 2007.

[22] N. Behdad and K. Sarabandi, “A wide-band slot antenna design employing a fictitious short circuit concept,” IEEE Trans. Antennas Propag., vol. 53, pp. 475–482, Jan. 2005.

[23] K. Wu and D. Deslandes and Y. Cassivi, "The substrate integrated circuits - a new concept for high-frequency electronics and optoelectronics," in TELSIKS, University of Nis, Serbia & Montenegro, 2003.

[24] C. A. Balanis, *Antenna Theory, Analysis and Design,* 3rd ed. Hoboken, NJ: Wiley, 2005.